Nano Today (2016) xxx, xxx—xxx

Available online at www.sciencedirect.com

ScienceDirect

journal homepage: www.elsevier.com/locate/nanotoday

REVIEW

Electrode surface engineering by atomic layer deposition: A promising pathway toward better energy storage

Bilal Ahmed [1], **Chuan Xia** [1], **Husam N. Alshareef** *

Materials Science and Engineering, King Abdullah University of Science and Technology (KAUST), Thuwal 23955-6900, Saudi Arabia

Received 13 February 2016; received in revised form 13 March 2016; accepted 4 April 2016

KEYWORDS
ALD;
LIBs;
NIBs;
Supercapacitors;
Anode;
Cathode

Summary Research on electrochemical energy storage devices including Li ion batteries (LIBs), Na ion batteries (NIBs) and supercapacitors (SCs) has accelerated in recent years, in part because developments in nanomaterials are making it possible to achieve high capacities and energy and power densities. These developments can extend battery life in portable devices, and open new markets such as electric vehicles and large-scale grid energy storage. It is well known that surface reactions largely determine the performance and stability of electrochemical energy storage devices. Despite showing impressive capacities and high energy and power densities, many of the new nanostructured electrode materials suffer from limited lifetime due to severe electrode interaction with electrolytes or due to large volume changes. Hence control of the surface of the electrode material is essential for both increasing capacity and improving cyclic stability of the energy storage devices.

Atomic layer deposition (ALD) which has become a pervasive synthesis method in the microelectronics industry, has recently emerged as a promising process for electrochemical energy storage. ALD boasts excellent conformality, atomic scale thickness control, and uniformity over large areas. Since ALD is based on self-limiting surface reactions, complex shapes and nanostructures can be coated with excellent uniformity, and most processes can be done below 200 °C. In this article, we review recent studies on the use of ALD coatings to improve the performance of electrochemical energy storage devices, with particular emphasis on the studies that have provided mechanistic insight into the role of ALD in improving device performance.

* Corresponding author. Tel.: +966 128084477.
E-mail address: husam.alshareef@kaust.edu.sa (H.N. Alshareef).
[1] These authors contributed equally.

http://dx.doi.org/10.1016/j.nantod.2016.04.004
1748-0132/

Introduction

The increasing demand for portable electronics, electric vehicles, and large-scale grid storage requires efficient and environment friendly energy storage technologies with high energy and power densities and excellent life time [1–4]. Electrochemical energy storage devices offer numerous advantages such as high efficiency, low cost, excellent reversibility, extended cyclic performance and environment friendly operation. The most commonly used electrochemical energy storage devices are Li ion batteries (LIBs), first commercialized by Sony in 1991, provide excellent life span and performance [5,6]. In addition, high energy density Li-sulfur batteries (LSBs) and Li-oxygen batteries (LOBs) have reaped research focus due to their high theoretical capacity and cost effectiveness [7–10]. Furthermore, Na ion batteries (NIBs) have garnered increasing research attention because of abundant sodium (Na) resources, lower materials cost, and identical ion transfer chemistries with LIBs [11,12]. Despite their lower energy density as compared to LIBs, NIBs are considered viable candidates for large-scale energy storage systems. On the other hand, though batteries can deliver high energy density, their power density is low. Hence, for applications requiring high power, electrochemical capacitors, including electrical double-layer capacitors (EDLCs) and pseudocapacitors, are preferred [13–17].

Since the performance of energy storage devices largely depends on the choice of electrode materials, it is desirable to design and develop new materials with favorable electrochemical properties [18]. Recently, nanostructured materials have shown promise in energy storage applications due to various attractive properties. For instance, in LIBs, nanostructured anode and cathode materials provide short diffusion paths, large surface area, and can accommodate volumetric changes during charge/discharge process [19]. The synthesis of nanostructured materials has been carried out by different chemical and physical methods such as hydrothermal growth, electrodeposition, chemical vapor deposition and sol–gel. In addition, some of these techniques are used for making composites such as the hydrothermal process has been reported for preparing composites of graphene with different oxides and/or sulfides, providing improved performance in supercapacitors and batteries. Since electrochemical energy storage strongly depends on surface reactions at the electrolyte/electrode interface, an alternate approach to enhance electrode material performance is to passivate the electrode surface with appropriate layers. These surface passivation layers can be deposited by numerous methods such as sol–gel method [20] or chemical vapor deposition technique [21]; however, these techniques lack precise control over layer thickness, surface coverage, uniformity of coating, and they often require high temperature.

In recent years, atomic layer deposition (ALD) has emerged as powerful technique to deposit conformal coatings of different materials with excellent thickness control and conformality by using sequential surface chemical reactions. The prime application for ALD has been microelectronics, however as the technology has matured significantly, it is being considered for a variety of applications such as solar cells and catalysts. The implementation of ALD in electrochemical energy storage devices is rather recent topic, but it is already showing promising results. In LIBs, for example, ALD has been used to fabricate electrochemically active electrode materials, to prepare composites of different electrode materials, to deposit solid state electrolyte, and to modify electrode/electrolyte interface.

In energy storage devices, ALD offers advantages such as conformal coatings of complex structures, uniformity over large surface area, excellent control over thickness of deposited layer, and making composite nanostructures. The unique coating mechanism of ALD facilitates the electrode surface engineering according to customized requirements. For instance, the deposition of thin layer on electrode/electrolyte interface ensures the ionic diffusion and compensates volumetric changes during charge/discharge process. In addition, complex 2D and 3D nanostructures can be fabricated with ease. These features make ALD a promising solution to the problems of next generation energy storage devices. One potential drawback of ALD could be the cost of the system operation and precursor materials. However, these costs should drop as ALD becomes more pervasive. Another potential drawback could be in conventional electrode making process, where binder and conductive carbon are added to the active cathode or anode material. The multicomponent nature of such electrodes affect the uniformity of the ALD coating process. Another potential compromise is that the ALD process is inherently slow, so thick coatings such as solid-state electrolytes will require significantly more time than other deposition processes. Hence, in this article, we briefly review the ALD technique and its recent application in Li ion batteries, Li sulfur batteries, Li oxygen batteries, Na ion batteries and supercapacitors. We have categorized the ALD's application based on the function of the deposited ALD layer. Further, our review focuses on studies that have provided mechanistic insight into the role of ALD coatings, and provides overview of the future directions and prospects of this emerging topic in energy storage.

Atomic layer deposition — Overview

Atomic layer deposition (ALD) is a vapor-phase deposition technique, first proposed by Suntola and Antson in 1970 [22]. Initially, the application of ALD was limited to the semiconductor industry for synthesis of Group III-V and II-VI compounds [23,24]. However, in recent years, ALD has shown promise in various emerging fields such as solar cells and energy storage devices.

Although alternative methods such as chemical vapor deposition (CVD), physical vapor deposition (PVD) and electrodeposition can be used to deposit coatings for electrochemical devices fabrication, they are not as versatile as ALD. For instance, electrodeposition requires very conducting surfaces to deposit coatings, while ALD can coat conducting and non-conducting surfaces. Furthermore, unlike CVD and PVD, ALD is a surface controlled process where film growth is controlled by self-terminating gas-solid

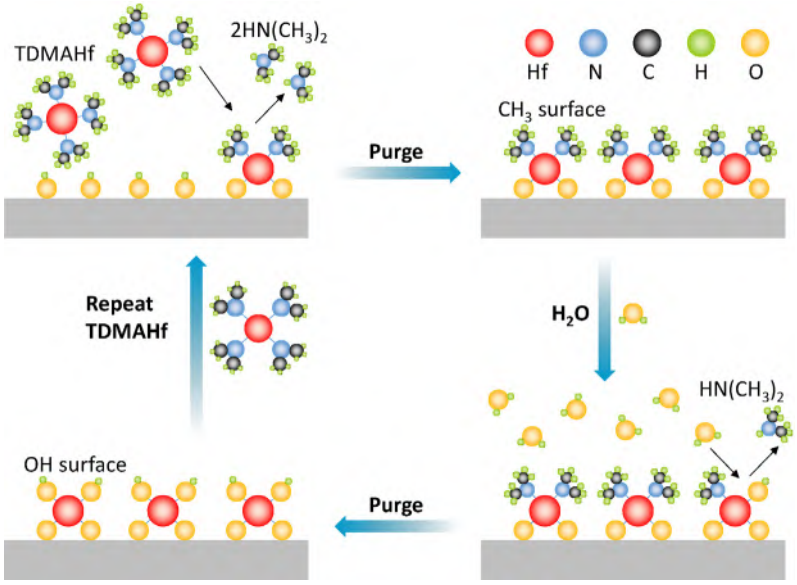

Figure 1 Schematic representation of the reaction process in atomic layer deposition of HfO_2. The illustrated process uses $Hf(N(CH_3)_2)_4$ (TDMAHf) as precursor and H_2O as oxidant. ALD is an ideal platform for surface modification of electrode materials in stand-alone and on-chip energy storage devices. This is because it offers precise thickness control, very good uniformity, and excellent conformality regardless of the shape of current collector.

surface reactions. This gives excellent control over thickness and uniformity over large areas. The characteristics of deposited film largely depend on three factors: substrate type, deposition temperature, and precursor materials. The substrate should have sufficient number of reactive sites to facilitate the ALD growth [25,26]. The minimum deposition temperature for ALD process would be the one which minimizes the physisorption of precursor components [27] and maximum temperature would be the one which does not decompose the precursor. The ALD precursor should be able to generate enough concentrations of vapors in gaseous phase to saturate all the adsorption sites on substrate [28]. The unique mechanism of ALD growth offers advantages such as low growth temperatures (100—250 °C), atomic scale stoichiometric deposition, excellent conformality and thickness control as compared to other depositions techniques.

The basic features of the ALD growth process can be explained using HfO_2 as an example, as shown in the schematic in Fig. 1. Like any other binary ALD process, HfO_2 requires two precursors: hafnium (Hf) source and oxygen source. In our process, depicted in Fig. 1, tetrakis(dimethylamino) hafnium ($Hf(N(CH_3)_2)_4$) has been used as Hf source and H_2O as oxygen source. A hydroxylated surface is necessary to initiate the reaction. The Hf precursor reacts with chemisorbed hydroxyl (—OH) and produces two alkylamine molecules as by-products. In the second half reaction, H_2O replaces the other two alkylamine ligands to form a hydroxylated surface for the next cycle of reaction. The Hf—N bonds in the HfAA molecule are selectively cleaved by H_2O molecules. The dose time, reaction time and proper removal of access precursor are key factor defining quality and thickness control of deposited film. The deposition of HfO_2 is also possible from other precursors such as $HfCl_4$ and ozone.

ALD in energy storage devices

Efficient energy storage with high capacity and extended lifetime is critical for the realization of renewable energy systems and environment friendly electric vehicles. The spectrum of energy storage also includes the long-lasting portable electronic devices such as LIBs and electrochemical supercapacitors. LIBs are preferred due to their high energy density and extended life time, but their use in high power application is limited because of lower power densities [1,2]. On the other hand, electrochemical supercapacitors are preferred for high power density applications but are limited by the lower values of energy density. A number of approaches have been taken to increase the stability, energy density and power density of electrochemical energy storage devices. In this review, we focus on the recent trend of using atomic layer deposition (ALD) for this purpose. After a quick survey of the literature on the utilization of ALD for electrode surface engineering in energy storage applications, one realizes that ALD has been used to perform the various functions, which are summarized in Fig. 2. Electrode surface engineering in the context of this review refers to coating of the anode or cathode of an electrochemical device (e.g. Li ion batteries) with specific materials to achieve one or more of the following. Surface coatings should reduce the speed of undesired surface reactions such as those involved SEI layer formation to reduce capacity decay, cause minimal impact on diffusion of ions such as Li^+ and Na^+, and cause minimal drop in conductivity of the anode or cathode material. In addition, coatings should be mechanically compliant to accommodate large volume changes for conversion type electrodes. Engineering the battery electrode would involve carefully evaluating the properties of the coatings (e.g., structure, composition, thickness, microstructure, stability, conductivity, and mechanical properties) and picking the

Please cite this article in press as: B. Ahmed, et al., Nano Today (2016), http://dx.doi.org/10.1016/j.nantod.2016.04.004

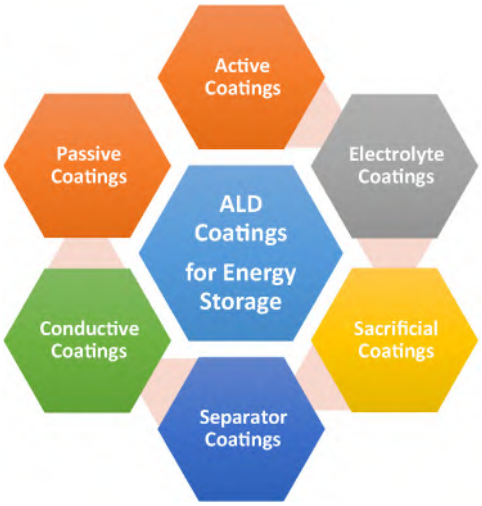

Figure 2 Different possible functions of ALD coatings in energy storage devices. One coating may also simultaneously perform different functions in the same device.

ones that are likely to achieve the desired effect. For example, coatings used to achieve better conductivity cannot be insulating themselves.

The categorization, given in Fig. 2, defines following roles for ALD coatings: active coatings, passive coatings, conductive coatings, separator coatings, electrolyte coatings and sacrificial coatings. Briefly, active coatings are used as electrode materials with novel architectures to increase capacity and life time. The passive coatings are designed to reduce the detrition of electrode material during charge/discharge process, ideally without hindering the diffusion of Li^+ or Na^+ ions in batteries, or degrading surface reactions in the case of electrochemical capacitors. The passive coatings themselves have little electrochemical activity. Conductive coatings, on the other hand, can help reduce the overall equivalent series resistance of the devices and hence increase their power density. For example, ALD has been utilized to prepare three dimensional conductive current collectors with complex geometries and novel designs. The separator coatings can be applied to the separator material to change its wetting behavior or to help with thermal management. Recently, solid electrolyte layers have also been deposited by ALD. Fig. 3 summarizes the benefits of each type of ALD surface coating (shown in Fig. 2).

Active coatings

Atomic layer deposition (ALD) has been widely used to deposit active layers of nanostructured electrode materials for batteries and supercapacitors. Due to the uniform and conformal nature of ALD, various 2D and 3D nanostructures have been reported in different battery systems. Table 1 summarizes literature on ALD prepared active coatings, which have been reported in secondary ion batteries.

Vanadium oxide was the first ALD prepared positive electrode material for Li ion batteries [29—38]. Lincot et al. has published several studies on using vanadium oxide as cathode material, explaining the V_2O_5 growth mechanism by in situ quartz crystal microgravimetry and electrochemical reactions by Raman spectroscopy [29—32,34]. The ALD process for the preparation of V_2O_5 films uses vanadyl triisopropoxide ($VO(OC_3H_7)_3$, VTOP) as the vanadium precursor and water as the oxidant, which yields amorphous films associated with V_2O_5 gel formation from water exposure in the process [29,34]. The authors showed that post annealing above 400 °C is required to remove the residual water and crystallize the films, which restricts the substrate choice. To overcome this problem, ozone based ALD process of crystalline V_2O_5 films has been developed and the resulted films showed improved performance in Li ion battery cathodes [35]. Furthermore, a 3D multiwall carbon nanotube (MWCNT) sponge network, coated by ALD V_2O_5 has been reported which delivers 450 times higher areal capacity than planar counterparts (816 μAh/cm^2 at 1C rate, voltage range: 2.1—4.0 V vs. Li/Li^+) [36]. This extraordinary performance improvement is due to the highly conductive nature of MWCNT, unprecedented uniformity of ALD thin film coatings, and high surface area and porosity of the MWCNT sponge material for ion transport. Fig. 4 shows

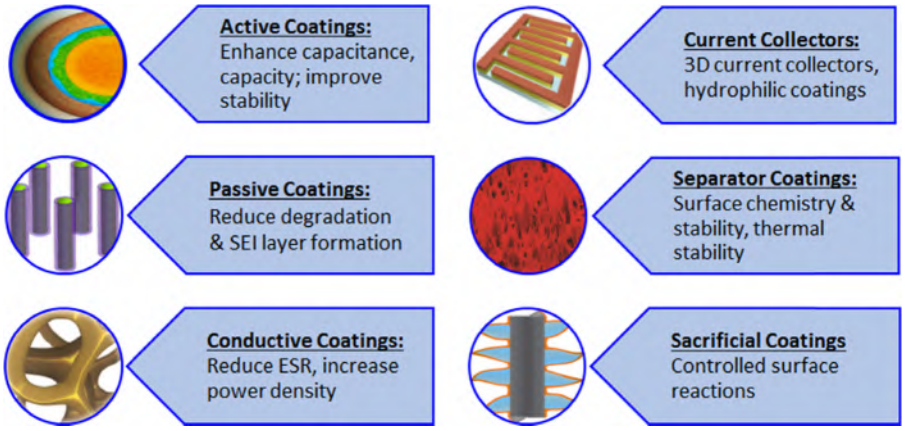

Figure 3 Summary of the potential benefits of the various types of ALD coatings that have been reported in energy storage devices, including batteries and electrochemical capacitors. It is possible that one coating layer may perform more than one function in the same energy storage device.

Table 1 ALD coating reported for Li ion batteries (LIBs), Na ion batteries (NIBs), Li-S batteries (LSBs) and Li-O_2 batteries (LOBs). The commonly used configuration is used in conventional Li ion batteries unless otherwise stated.

Function	ALD materials	Commonly used configuration	Ref.
Active coating (cathode)	V_2O_5	V_2O_5@SnO_2 coated glass, V_2O_5@Au coated SS Spacer and MWCNT/V_2O_5 Core/Shell Sponge	[29–38]
	$LiFePO_4$	$LiFePO_4$/CNTs	[41]
	$FePO_4$	$FePO_4$@N-doped CNTs	[40]
	$LiCoO_2$	$LiCoO_2$@TiO_2 coated Si	[39]
	Pd	Pd@Carbon (LOBs)	[42]
	Li_2S	Li_2S@Cu Foil (LSBs)	[43]
	TiO_2	TiO_2/Peptide structure, TiO_2 NTs, TiO_2/Ni/Tobacco Mosaic Virus, 3D Ni/TiO_2 NWs network, TiO_2@Graphene, 3D np-Au/TiO_2 coreshell, 3D TiO_2/C, SnO_2@TiO_2 double shell, ZnO@TiO_2 coreshell, TiO_2@Fe_2O_3, TiO_2@CNSs	[45,47,51–64]
Active coating (anode)	RuO_2	RuO_2/MWCNTs	[65]
	SnO_2	SnO_2/GNS, SnO_2/SS Substrate, SnO_2/Ni Foam	[44,46,55,59,60,66]
	GaS_x	GaS_x/SWCNTs	[48,49]
	MoN_x	MoN_x/Stainless steel spacer	[50]
	WN_x	WN_x/Stainless steel spacer	[67]
	Cu_2S	Cu_2S/SWCNTs	[68]
	Co_3O_4	Co_3O_4/TiN/Si Substrate	[69]
	ZnO	ZnO@Graphene	[70]

the schematic of experimental flow used to fabricate V_2O_5 coated MWCNT sponges. ALD enables conformal coating of V_2O_5 on the highly porous MWCNT sponge. The coated MWCNT sponge was pressed and used as the cathode, where the MWCNT functions as an electron conductor, V_2O_5 functions as Li storage material, and the open pores allow easy electrolyte access. The thickness of the sponge was initially about 2000 μm, but was reduced to around 170 μm after compression to form a coin cell battery [36]. Apart from V_2O_5, lithiated cathodes such as $LiCoO_2$ [39] $FePO_4$ [40] and $LiFePO_4$ [41] cathodes have been prepared by ALD process. Liu et al. [41] has deposited $LiFePO_4$ on functionalized CNTs using Fe_2O_3, PO_x and Li_2O sub-cycles and achieved stable cathode performance up to 2000 cycles. Same group has also reported the preparation of $FePO_4$/CNTs composite by combining Fe_2O_3 and PO_x sub-cycles and characterized as LIBs cathodes [40].

Apart from conventional LIBs, ALD is also being used in emerging Li ion systems such as Li–O_2 batteries (LOBs) and Li sulfur batteries (LSBs). Lei et al. has deposited nanostructured palladium (Pd) on porous carbon as the cathode material for Li–O_2 cells [42]. The conformal nature of ALD disperses the Pd catalyst onto the carbon support while preserving the initial porous structure and

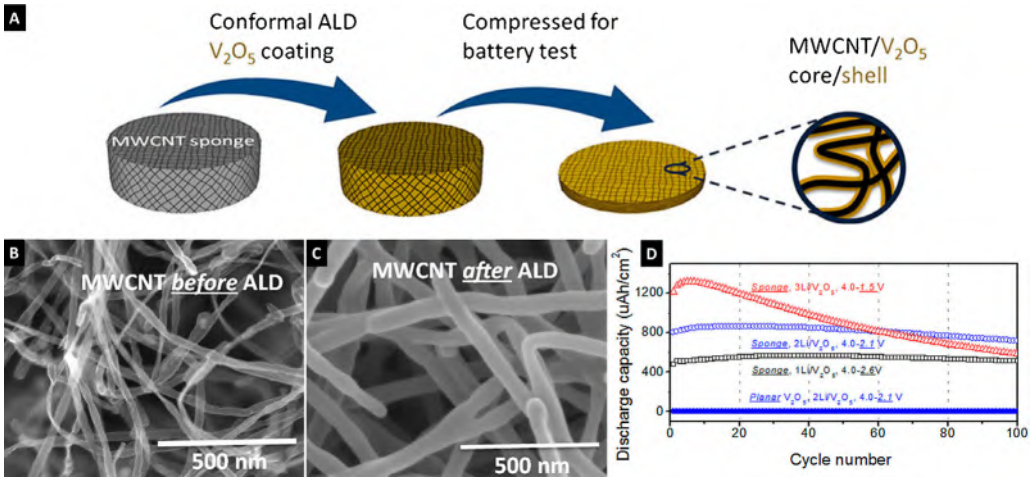

Figure 4 (A) Schematic of experimental flow to fabricate V_2O_5 coated MWCNT sponge. ALD enables conformal coating of V_2O_5 on the surface of the highly porous MWCNT sponge, (B) SEM images of MWCNT sponge before and (C) after 1000 cycles of ALD V_2O_5 coating, and (D) cyclic performance and areal capacity comparison between the cell with planar V_2O_5 cathode in the voltage range for 2Li/V_2O_5 (4.0–2.1V) and the cells with MWCNT/V_2O_5 sponge cathodes in three different voltages at 1C current.
Reprinted with permission from Chen et al. ACS Nano 6 (9) (2012) 7948–7955. Copyright 2012 American Chemical Society [36].

Please cite this article in press as: B. Ahmed, et al., Nano Today (2016), http://dx.doi.org/10.1016/j.nantod.2016.04.004

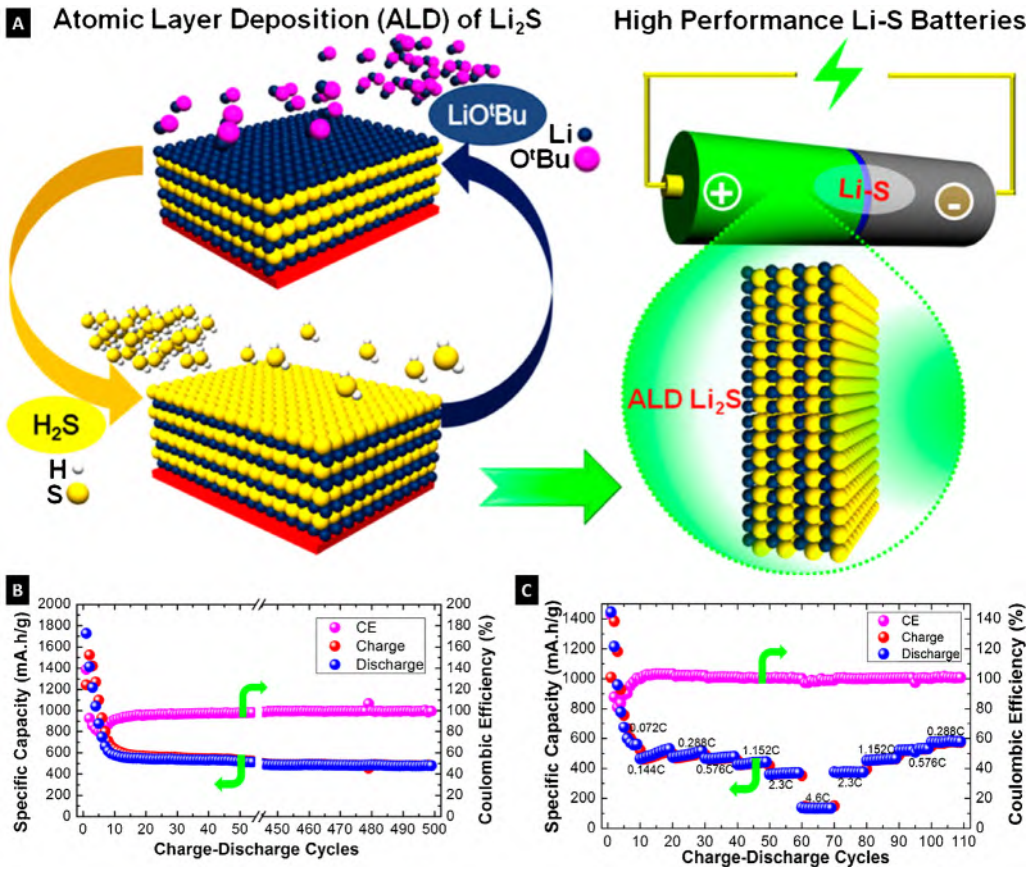

Figure 5 (A) Schematic illustration of ALD deposition of Li_2S and its application in Li-Sulfur batteries, (B) cyclic stability and (C) rate capability of Li_2S films deposited onto 2D planar Cu foils using 700 ALD Li_2S cycles at 200 °C.
Reprinted with permission from Meng et al., ACS Nano 8 (10) (2014) 10963−10972. Copyright 2014 American Chemical Society [43].

resulted in significant performance improvement of LOBs (≈6600 mAh/g at 100 mA/g). Another report [43] demonstrated the development of ALD process for Li_2S thin film and its utilization as cathode electrode in LSBs. The ALD Li_2S thin film exhibited a high specific capacity of up to 800 mAh/g, excellent cyclic performance and high Coulombic efficiency without using any electrolyte additives. Fig. 5 shows the excellent cyclic performance and rate capability of LSB along with schematic representation of ALD process.

On the other hand, the spectrum of ALD prepared anode materials for LIBs is wider, ranging from transition metal oxides to various sulfides and nitrides. SnO_2 and TiO_2 are typical examples of ALD prepared oxide anodes for Li ion batteries. The SnO_2 is a well-known anode material because of its high theoretical Li storage capacity (~781 mAh/g), but it suffers from large volumetric changes during charge/discharge process resulting in poor cyclic performance [44]. On the contrary, TiO_2 is preferred because of its excellent stability, however its electrical conductivity (4.97×10^{-11} S/m) limits its practical utilization [45]. ALD offers a unique solution to these problems by either constructing 3D nanostructures to sustain volumetric changes or preparing metal oxide/carbon (CNTs, graphene sheets, etc.) nanocomposite to overcome the conductivity issues.

One typical example of ALD prepared 3D nanostructure has been reported by Jacob et al., where an ultrathin film of amorphous SnO_2 has been deposited on a free standing 3D Ni foam [44]. ALD allows for the entire surface of the 3D current collector to be conformally coated with a thin film of uniform thickness, while the thickness of Ni foam maximizes the areal capacity. The stable specific capacity of 505 mAh/g and areal capacity of 0.54 mAh/cm^2 after 200th cycle was achieved at current density of 500 mA/g [44]. In another study, the composite of SnO_2 and graphene nanosheets (GNS) has been prepared by ALD [46]. The ALD process parameters are controlled to obtain different crystalline and amorphous phases of SnO_2 which were tested as anode material in LIBs. The amorphous SnO_2/GNS composites delivered a higher coulombic efficiency (≈100%), a high specific capacity (821 mAh/g@194th cycle) and superior cyclic stability [46]. The study concluded that improved performance of amorphous SnO_2/GNS composites is due to the isotropic nature of amorphous SnO_2, which can buffer the large volume expansion and shrinkage of the Sn lattice during the charge/discharge process.

Another way of constructing 3D nanostructure is utilization of a sacrificial template. Kim et al. reported a 3D network of TiO_2 hollow nanoribbons designed from a peptide assembly using ALD [45]. The well connected network of nanoribbons and the hollow structure of each nanoribbon improved the transport properties of Li ions and electrons. Fig. 6 shows the schematic representation of TiO_2 formation by ALD process, corresponding SEM image, and rate performance when used as anode material. The

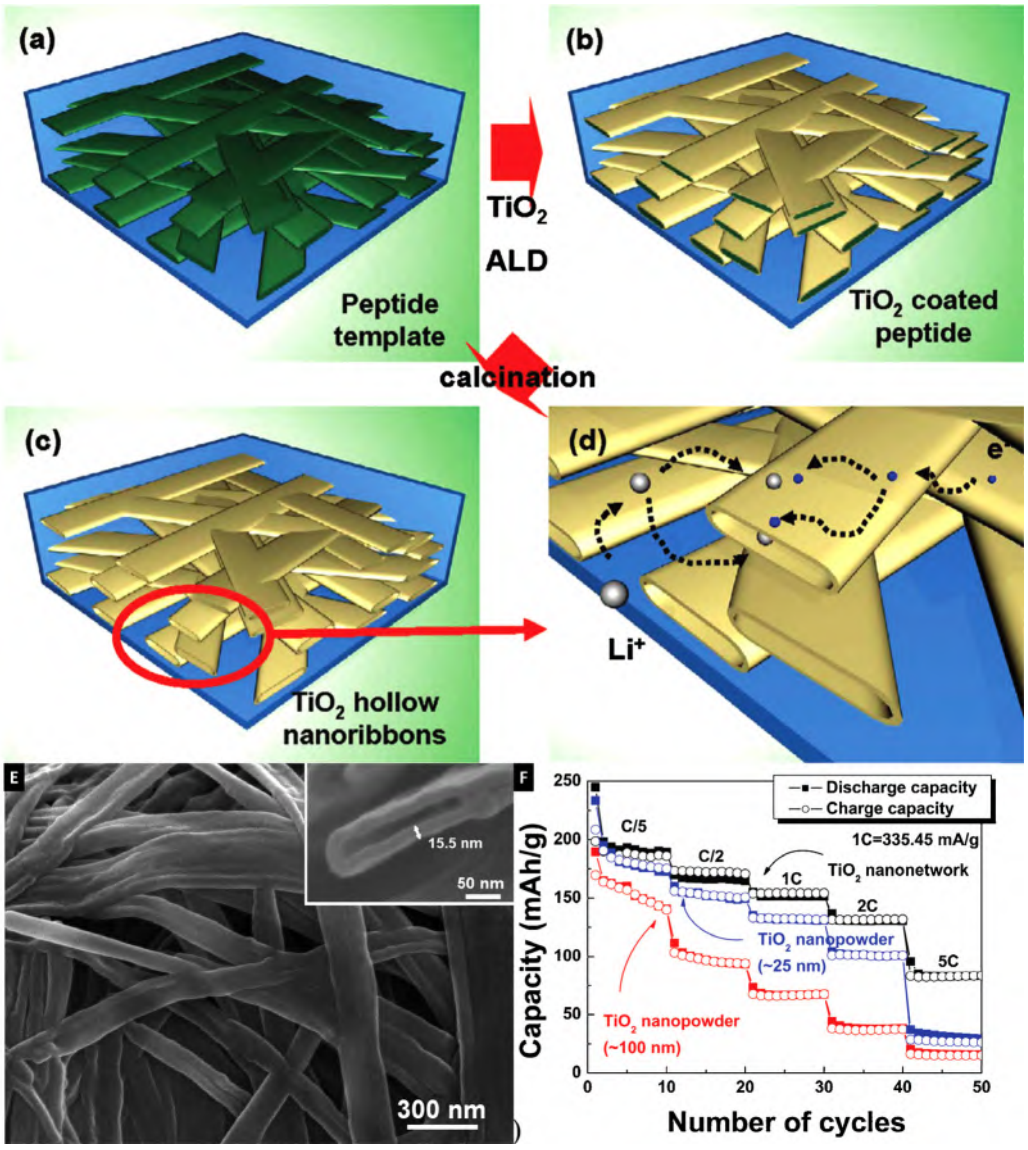

Figure 6 Schematic illustration of (a) the 3D peptide template, (b) atomic layer deposited TiO_2 on the peptide template, (c) 3D network structure of TiO_2 hollow nanoribbons, (d) the Li^+ ions and electrons transport in the TiO_2 nanonetwork electrode, (E) FESEM images of the TiO_2 nanonetwork (inset: magnified image of cross sectional TiO_2 hollow nanoribbon) and (F) rate capability of the TiO_2 nanonetwork, the 25 nm and 100 nm TiO_2 nanopowders from C/5 to 5C for 10 cycles.
Reprinted with permission from Kim et al., ACS Nano 3 (5) (2009) 1085—1090. Copyright 2009 American Chemical Society [45].

fabrication of highly ordered network structure of TiO_2 nanoribbons demonstrated excellent electrochemical performance in terms of specific capacity, rate capability, and cyclic performance because of structural integrity and superior ionic/electronic conductivity [45]. Furthermore, Wang et al. has successfully fabricated 3-D Ni/TiO_2 nanowire network based on a 3-D porous anodic alumina template-assisted electrodeposition and ALD processes [47]. The 3D Ni/TiO_2 nanowire network showed higher areal capacity as compared to Ni/TiO_2 nanowire arrays fabricated using conventional porous anodic alumina templates. The 100% capacity is retained after 600 cycles due to the stable Ni/TiO_2 nanowire network structure. Apart from these representative studies, other demonstrated configurations of TiO_2 and SnO_2 can be found in Table 1.

Besides transition metal oxides, different sulfides and nitrides have also been studied as anode materials for LIBs. However, the major research is focused on development of ALD processes for different sulfide material. For instance, gallium sulfide (GaS_x) films were deposited by ALD, using alternating exposures to $Ga_2(NMe_2)_6$ and H_2S in the temperature range of 125—225 °C [48]. The films are smooth, amorphous, and conformal on high-aspect-ratio substrates. The resultant ALD GaS_x films exhibited excellent electrochemical performance as a LIB anode, showing high capacity and reliable cyclic stability, compared to commercial Ga_2S_3 [48,49]. Similarly, ALD process for molybdenum nitride (MoN_x) films using molybdenum hexacarbonyl and ammonia has been demonstrated by Nandi et al. [50]. The as-grown thin films demonstrated notable potential as a

Table 2 Summary of recent ALD studies on electrochemical capacitors.

Function	ALD material	Commonly used configuration	Ref.
Active coatings	TiN	TiN on Graphene sheet; TiN on porous silicon, C@TiN-AAO	[71—73]
	RuO_2	RuO_2 on rGO; RuO_2 on CNT; RuO_2 on bio-template	[74,84,85]
	TiO_2	TiO_2 on Vertically-Aligned Carbon Nanotube; TiO_2 on CNT; TiO_2 on Graphene	[75—77]
	VO_x	VO_x on CNT, VO_x on Al NW	[78,79]
	NiO	NiO on GF-CNT; NiO on nanoporous graphene	[80,81]
	Fe_2O_3	Fe_2O_3 on carbon nanotubes/carbon cloth	[86]
	Fe_2N	Fe_2N on Graphene nanosheet	[71]
	Co_3O_4	Co_3O_4 on carbon nanotubes/carbon cloth	[82]
	Co_9S_8	Co_9S_8 on Ni Foam	[83]
Passive coatings	Al_2O_3	Al_2O_3 on Carbon; Al_2O_3 on Cellulose fiber	[87,88]
	RuO2	RuO_2 on PANi	[89]
Sacrificial coatings	TiO_2	TiO_2 on NiO; TiO_2 on CoO	[90]
	Al_2O_3	Al_2O_3 on $Ni_xCo_{1-x}O$; Al_2O_3 on Co_3O_4; Al_2O_3 on CoO	[91—93]
	SnO_2	MnO_2@SnO_2-AAO	[94]
Conductive coatings	Pt	MnO_2@Pt-Al foil	[95]
	TiN	MnO_2@TiN-AAO	[96]

carbon and binder-free anode materials in a LIBs. Under half-cell configuration, a stable discharge capacity of 700 mAh/g was achieved after 100 charge/discharge cycles, at a current density of 100 $\mu A/cm^2$ [50].

In addition to batteries, ALD has been also utilized in electrochemical supercapacitors to prepare active coatings and published literature has been summarized in Table 2. ALD has been demonstrated to conformally coat electrochemically active nanomaterials on high-surface-area support (e.g. aligned graphene/CNT nano-forests) to improve active material properties like poor electrical conductivity, instability, and so on. Current research showed metal oxides (RuO_x, TiO_2, VO_x, NiO, Co_3O_4), nitrides (TiN), and sulfides (Co_9S_8) could be uniformly deposited by ALD on the current collector to form a binder free cathode electrode [71—83].

In one example, the electrochemical capacitive properties of ALD prepared ruthenium oxide (RuO_2) on vertically aligned carbon nanotube (CNT) forests (Fig. 7a and b) have been investigated by Lin and co-workers [74]. As shown in Fig. 7c, 100 and 170 times higher specific capacitance after ALD coating and after further electrochemical oxidation was achieved, respectively, as compared to pure CNT support. More interestingly, the measured capacitance value was close to the theoretical limit of RuO_2 at 644 F/g with a high power density at 17 kW/kg. A similar approach was also illustrated by Yang et al. [84]. They have deposited small amounts of RuO_2 on reduced graphene oxide (rGO) by ALD. Such a RuO_2/rGO electrode offered a specific capacitance of 1132 F/g at 50 mV/s, which is very close to the theoretically achievable value. Furthermore, the cycling stability of the electrodes has been significantly improved. After 4000 continuous cycles, ~92% of initial capacitance was retained. Besides, as illustrated in Fig. 7(d—f), Wang's group has developed a vapor-phase ALD process for one-step conformal deposition of high quality metal sulfides (Co_9S_8) on high aspect-ratio 3D nanostructures using bis(N,N′-diisopropylacetamidinato)cobalt(II) and H_2S as precursors. Deep trenches with an aspect ratio of 10:1 were demonstrated [82]. When evaluated as supercapacitor cathode, this Co_9S_8/Ni Foam integrated electrode was able to deliver excellent specific capacitances of 1645 and 1309 F/g (Fig. 7g) at the current densities of 3 and 45 A/g, respectively. This impressive rate capability was achieved due to the high conductivity and ultra-thin nature of ALD-prepared active materials, so that the ion diffusion length and the charge transfer length were both minimized. No obvious decay in capacity was found for this binder-free cathode and the capacity remained at 94.4% of its initial value after 2000 cycles at a high current density of 45 A/g (Fig. 7h).

On the other hand, Fe_2O_3, TiN and Fe_2N based supercapacitor anodes were also successfully prepared by ALD technique. For instance, Guan and co-workers reported a promising supercapacitor anode by developing a hierarchical graphite foam-carbon nanotube framework (GF-CNT) and coating the surface with a thin layer of iron oxide [86], as shown in Fig. 8a. They found that the mass loading of Fe_2O_3 was an important parameter in determining the capacitance of the hybrid electrode (Fig. 8b). The best electrochemical performance was achieved in GF-CNT@400Fe_2O_3 sample, where ~470.5 mF/cm^2 was achieved at 20 mA/cm^2 which is ~4 times larger than that of pure carbonaceous substrate with a rate retention of 63.8% from 5 to 40 mA/cm^2. As shown in Fig. 8c, when combined with $CoMoO_4$ cathode, the optimized cell exhibited a high energy density of ~74.7 Wh/kg at the power density of ~1.4 kW/kg. In a recent study, Fan's group reported the fabrication of Fe_2N nanoparticle on vertically aligned graphene nanosheets (GNS) substrate as supercapacitor anode [71]. Their process is briefly described in Fig. 8d. To be specific, they, firstly, deposited ZnO thin film on GNS support by ALD; then the anode precursor (FeOOH) was obtained via a facile solution reaction from ZnO thin film. Next, Fe_2N nanoparticle was transferred from as-prepared precursor by ammonia annealing. As shown in Fig. 8e, the GNSs homogeneously cover

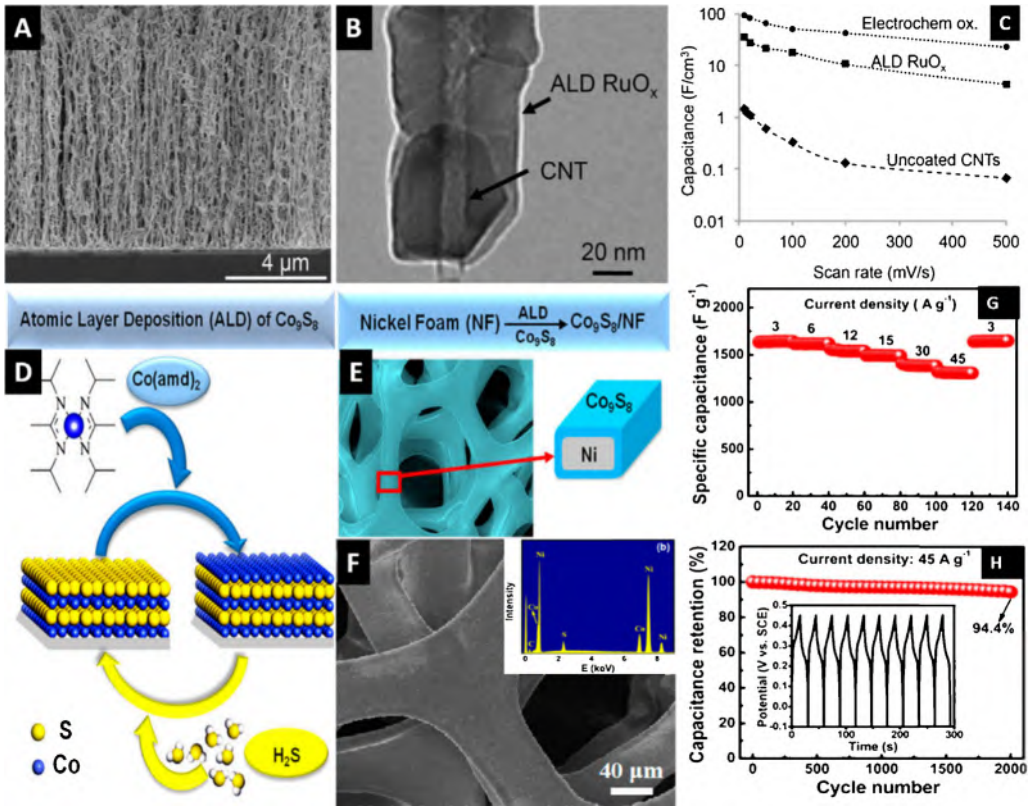

Figure 7 (A) SEM image of vertically aligned CNTs coated with ALD RuO_x. (B) TEM image of a single CNT conformally coated with ALD RuO_x. (C) Capacitance of uncoated CNT, as-deposited ALD RuO_x/CNT, and electrochemically oxidized ALD RuO_x-CNT electrodes at scan rates of 10 mV/s to 500 mV/s. (D and E) Schematic of the deposition route of Co_9S_8 on Ni foam. (F) SEM image Co_9S_8/Ni foam electrode. Inset in panel (F) shows an image of the EDS spectrum of Co_9S_8/Ni foam. (G and H) Electrochemical performance of as-prepared hybrid electrode. Panels (A—C) are reproduced from [74] with permission from The Royal Society of Chemistry. Panels (D and F) are reproduced with permission from Li et al., Nano Lett. 15 (10) (2015) 6689—6695. Copyright 2015 American Chemical Society [83].

the surface of carbon fibers, and porous Fe_2N nanoparticle were also homogeneously covered/distributed on the thin GNS. Owing to the high electrical conductivity of both electroactive materials and substrate, the maximum usage of the substrate surface and tight physical connection of both metal nitride materials with the GNS current collector, these samples exhibited a specific capacitance of around 170 F/g at 10 mV/s with a capacitance retention of ~77% from 10 to 100 mV/s (Fig. 8f). This report demonstrates that the strategy of combining ALD with ammonia annealing can be generally extended to other metal nitrides such as SnN, AlN, Zn_3N_2, and Mg_3N_2 for electrochemical energy storage applications.

Passive coatings

The interfacial reactions occurring between electrode and liquid electrolyte during charge/discharge process play critical role in determination of battery performance and cyclic stability. For instance, the formation of a stable solid electrolyte interface (SEI) is desirable for high columbic efficiency and cyclic performance because it prevents the decomposition of organic electrolytes and further consumption of Li^+ ions [97]. On the other hand, HF generated in the electrolytes during charge/discharge process deteriorates the electrode nanostructure and results in rapid performance degradation. This realization leads to the fact that interfaces designed and tailored according to the degradation mechanism will be beneficial for battery performance [97].

For this purpose, surface modification of electrode materials with passive coatings (coatings that are not electrochemically active themselves) has been carried out by numerous methods such as chemical vapor deposition (CVD), hydrothermal treatment or sol—gel processes [20,21]. In order to effectively improve battery performance, the passive surface coatings should have following properties: (1) minimal thickness, but with good uniformity, (2) good electronic and/or ionic conductivity, and (3) ability to accommodate volumetric changes during charge/discharge process (sometimes referred as toughness). Despite the wide variety of coating material choices, the above mentioned conventional techniques lack control over thickness and uniformity that can be available from ALD [98]. The ALD-based passive coatings have been therefore studied for the anode/electrolyte interface and the cathode/electrolyte interface. The most commonly used ALD passive coatings on battery electrodes are summarized in Table 3.

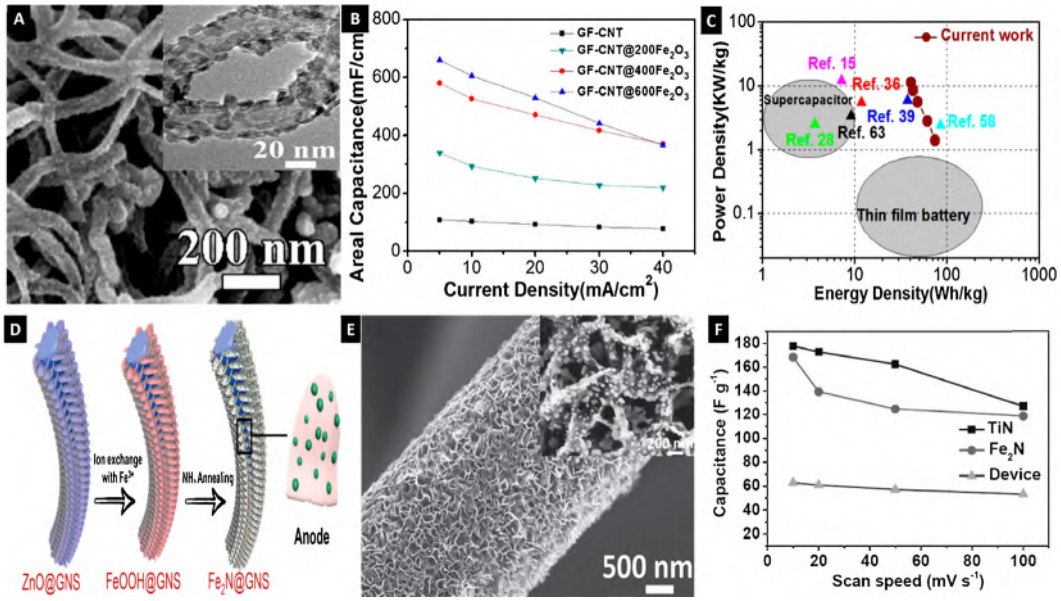

Figure 8 (A) Typical SEM image of as-synthesized Fe_2O_3 decorated hierarchical graphite foam-carbon nanotube framework. (B) Specific capacitance of various Fe_2O_3/GF-CNT electrode vs. current densities. (C) Ragone plot of the GF-CNT@Fe_2O_3//$CoMoO_4$ full cell. (D) Schematics of the fabrication processes of metal nitride anode materials. (E) SEM image of GNS grown on carbon fiber. The inset images shows that the Fe_2N nanoparticles are homogenously covered on graphene sheets. (F) Electrochemical performance of Fe_2N/GNS integrated electrode. Panels (A—C) are reproduced with permission from Guan et al., ACS Nano 9 (5) (2015) 5198—5207. Copyright 2015 American Chemical Society [86]. Reprinted with permission from Zhu et al. Advanced Materials, 2015, 27 (31), 4566—4571. Copyright 2015 John Wiley & Sons, Inc. [71].

Se-Hee Lee's group was the first to apply ALD for interface modification by passive layers in Li ion batteries. In 2010, his group demonstrated that a nanoscale layer of Al_2O_3, deposited by ALD, on the most commonly used LIBs cathode, nano-$LiCoO_2$, results in excellent cyclic stability, durable high energy and remarkable rate performance [104]. The coated nano-$LiCoO_2$ electrodes with 2 ALD cycles delivered a discharge capacity of 133 mAh/g with currents of 1400 mA/g

Table 3 ALD fabricated passive coatings in Li ion batteries (LIBs), Na ion batteries (NIBs), Li-S batteries (LSBs) and Li-O_2 batteries (LOBs). The commonly used configuration is used in conventional Li ion batteries unless otherwise stated.

Function	ALD materials	Commonly used configuration	Ref.
Passive coating (cathode/electrolyte interface)	Al_2O_3	Al_2O_3@$LiCoO_2$, $Li(Li_{0.2}Mn_{0.54}Ni_{0.13}Co_{0.13})O_2$, $Li(Ni_{1/3}Mn_{1/3}Co_{1/3})O_2$, $LiNi_{0.5}Mn_{1.5}O_4$, V_2O_5, $LiMn_2O_4$, $Li_{1.2}Ni_{0.15}Mn_{0.55}Co_{0.1}O_2$, $LiNi_{0.5}Mn_{1.5}O_4$	[99—120]
	TiO_2	TiO_2@$LiCoO_2$, $LiNi_{0.5}Mn_{1.5}O_4$, $Li_{1.2}Ni_{0.13}Mn_{0.54}Co_{0.13}O_2$, $LiMn_2O_4$	[105,112,117]
	CeO_2	CeO_2@$LiMn_2O_4$	[121]
	ZrO_2	ZrO_2@$LiMn_2O_4$ and $LiCoO_2$	[113,117,122—124]
	ZnO	ZnO@$LiMn_2O_4$, $LiMn_2O_4$/Graphene, $LiNi_{0.5}Co_{0.2}Mn_{0.3}O_2$,	[105,113,125,126]
	AlW_xF_y	AlW_xF_y@$LiCoO_2$	[127]
	FeO_x	FeO_x@Carbon (LOBs)	[128]
Passive coating (anode/electrolyte interface)	Al_2O_3	Al_2O_3@Graphite, MoO_3, $Li_4Ti_5O_{12}$, Silicon, Fe_3O_4, CNTs, CNFs, Si/Graphene, Fe_2O_3, MnO, SnO_2, ZnO/Graphene, Cu_3Si, Li metal (LSBs), 2,5-Dihydroxy-1,4-benzoquinonedisodium salt (DHBQDS) (NIBs), MoO_{3-x}, $Na_2C_8H_4O_4$ (NIBs), S/Carbon (LSBs)	[99,110,111,129—161]
	TiO_2	TiO_2@ZnO, Graphite, Silicon, SnO_2, CNTs, MoS_2 (NIBs)	[138,146,147,162—167]
	HfO_2	HfO_2@SnO_2, MoO_3, MoS_2 (NIBs)	[168—170]
	TiN	TiN@Silicon	[171]
	ZrO_2	ZrO_2@$Li_4Ti_5O_{12}$	[172]
	ZnO	ZnO@Silicon, Graphene/Sulfur composite for LSBs	[158,173]
	MgO	MgO@ Graphene/Sulfur composite for LSBs	[158]

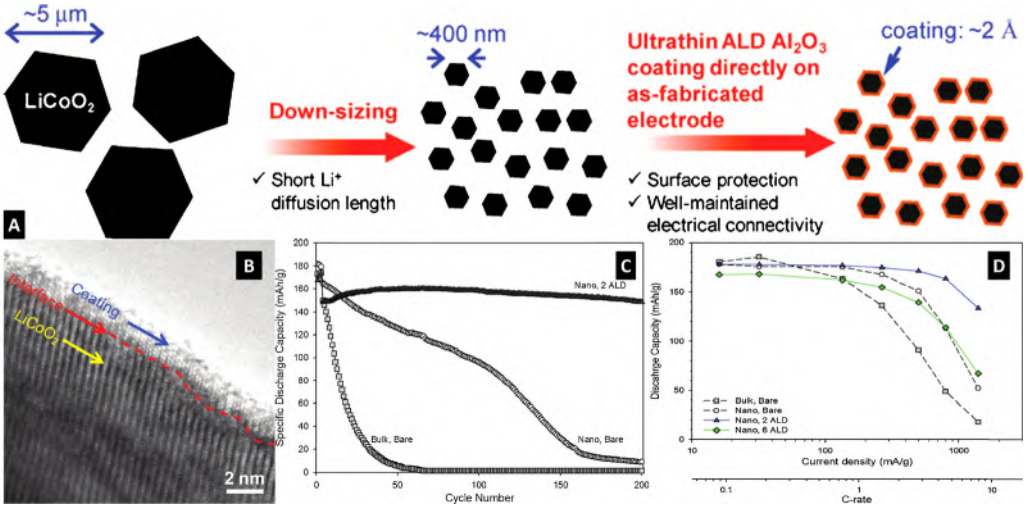

Figure 9 (A) Schematic representation of preparation of nanosized $LiCoO_2$ powder and ALD deposition, (B) the Al_2O_3 coated nano-sized $LiCoO_2$ particles by 6 ALD cycles on the bare powders, (C) cyclic performance of the electrodes: bare bulk $LiCoO_2$, bare nano-$LiCoO_2$ and Al_2O_3 coated nano-$LiCoO_2$ and (D) rate capability of the $LiCoO_2$ electrodes as a function of particle size and Al_2O_3 thickness. Reproduced with permission from Scott et al., Nano Lett. 11 (2) (2011) 414–418. Copyright 2011 American Chemical Society [104].

(7.8C), corresponding to a 250% improvement in reversible capacity compared to bare nanoparticles of $LiCoO_2$, when cycled at same current density. Fig. 9 shows that as prepared $LiCoO_2$ was down-sized to a nanoscale powder for short Li^+ ion diffusion lengths, followed by deposition of an ultrathin Al_2O_3. The deposition of an ultrathin Al_2O_3 layer on crystalline $LiCoO_2$ has been demonstrated in Fig. 9b. Fig. 9c shows the rate capability of the $LiCoO_2$ electrodes as a function of particle size and Al_2O_3 ALD-coating thickness. The Al_2O_3 coated nano-$LiCoO_2$ electrodes demonstrated a discharge capacity of 133 mAh/g at 7.8C which corresponds to a 250% improvement in reversible capacity compared to bare nano-$LiCoO_2$ electrodes (Fig. 9d). The precursors utilized for Al_2O_3 deposition in this study were trimethylaluminum (TMA, 97%) and H_2O and the two self-limiting surface reactions are given as follow:

$$AlOH^* + Al(CH_3)_3 \rightarrow AlO{-}Al(CH_3)_2{}^* + CH_4$$

$$AlO{-}Al(CH_3)_2{}^* + H_2O \rightarrow AlO{-}Al{-}OH^* + CH_4$$

The same group has reported that Al_2O_3 can be deposited on micrometer-sized $LiCoO_2$ and natural graphite by ALD to enhance durability and safety of LIBs. One of the important parameter in this type of electrode surface engineering is whether passive layer is deposited on powder or the prepared electrode? Same group has studied the difference between direct and indirect ALD coating and it has been shown that direct coating is more advantageous because of it conformity and full coverage [99]. Apart from Al_2O_3, other ALD coatings have been reported for different cathode materials. For instance, ultrathin and highly-conformal ZrO_2 coatings have been deposited on $LiMn_2O_4$ nanoparticles using ALD, which led to a remarkably enhanced high-rate electrochemical performance of $LiMn_2O_4$ cathode at elevated temperature [123]. Similarly, TiO_2 has been deposited on $LiCoO_2$, $LiMn_2O_4$ and $LiNi_{0.5}Mn_{1.5}O_4$ and demonstrated profound performance improvements [105,112,117,118].

Li et al. has compared the TiO_2, Al_2O_3 and ZrO_2, deposited by ALD, for Co dissolution in $LiCoO_2$ cathode system [117]. They have concluded that various metal oxide coating layers have different influences on the cycling performance and the rate capability of $LiCoO_2$ electrode. The Al_2O_3 coating effectively improved the electrochemical stability and showed excellent cyclic performance. They suggested the key parameters effecting the electrochemical performance can be summarized as (1) electrical conductivity, (2) electronic band structure, (3) suppression of the phase transition, (4) fracture toughness, and (5) scavenging HF species from the electrolyte [117].

ALD passive coatings have also been applied on anode/electrolyte interface to counter volumetric expansion effects and material degradation during charge/discharge process. Similar to cathode/electrolyte interface, ALD Al_2O_3 is the most studied material for anode/electrolyte interface as well. Jung et al. have deposited ultrathin layer of Al_2O_3 on natural graphite and studied the difference between direct vs. indirect coating [99]. They have concluded that when Al_2O_3 is deposited on powder, the insulating nature of Al_2O_3 hinders the electronic movement from natural graphite to current collector. Furthermore, despite the relatively low volumetric changes of natural graphite (≈14%), a slight change in volume severely disrupts the electrical connection. Therefore, the direct ALD coating on prepared electrode instead of powder is more advantageous [99]. On the anode side, ALD is mostly used for the materials showing high volumetric expansions during charge/discharge process such as MoO_3, iron oxide (Fe_2O_3 or Fe_3O_4), SnO_2, Si and MoS_2 etc. Kang et al. has prepared Fe_3O_4 nanoparticles confined in mesocellular carbon foam (MSU-F-C) and passivated by ALD Al_2O_3 [133]. David Mitlin's group has reported surface passivation of Si nanowire anode with different ALD materials

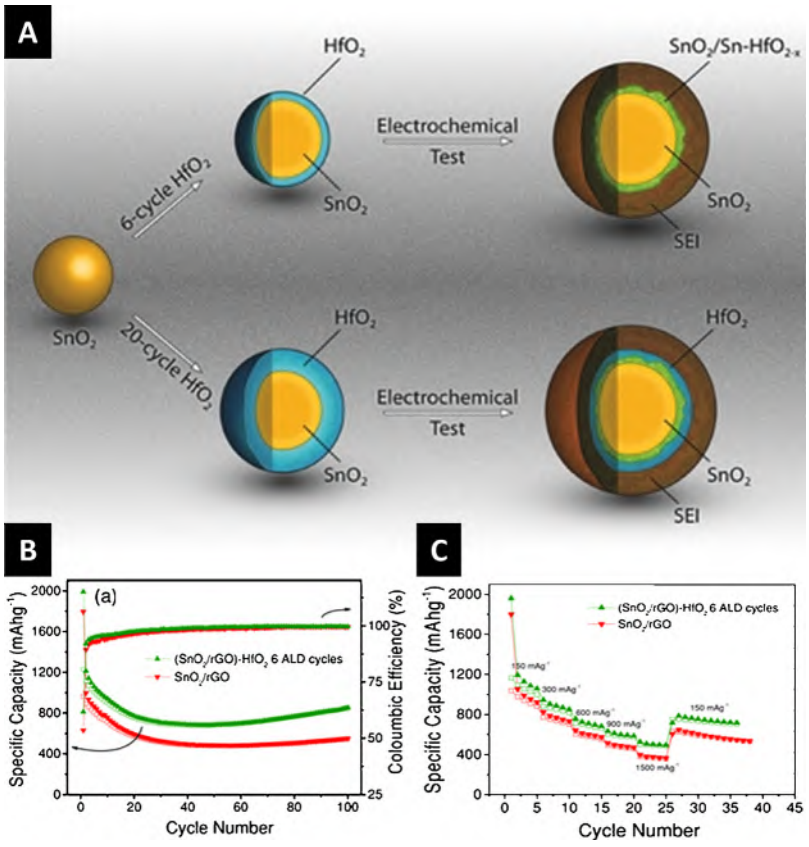

Figure 10 (A) Schematic illustration of ALD HfO_2 coated SnO_2 nanospheres, (B) cyclic performance of SnO_2/rGO and HfO_2 coated SnO_2/rGO electrodes at 150 mA/g and (C) rate capability at different current densities from 150 mA/g to 1500 mA/g. Reprinted with permission from Yesibolati et al. Small 10 (14) (2014) 2849–2858. Copyright 2014 John Wiley & Sons, Inc. [170].

such as Al_2O_3, TiO_2 and TiN [137,146,164,171]. The effect of coating on different morphologies and configurations has been studied and characterized in detail.

Apart from these conventional oxide materials, our group has reported HfO_2 as an alternative passivation layer. In 2014, Yesibolati et al. reported that ALD coating of HfO_2 on SnO_2 nanospheres can significantly enhance the cyclic performance and rate capability [170]. Ultrathin HfO_2 films were directly deposited on the prepared electrodes at elevated temperature (180 °C). The HfO_2 ALD reaction sequence was: (1) N_2 dose to 20 psi; (2) H_2O dose for 0.015 s; (3) H_2O reaction time 10 s; (4) Tetrakis(dimethylamino) hafnium ($Hf(NMe_2)_4$) dose to 0.2 s; (5) $Hf(NMe_2)_4$ reaction time 15 s (see Fig. 1). This sequence constitutes one cycle of ALD HfO_2 and the growth rate per cycle is 1.01 Å/cycle at these parameters. The results indicate that HfO_2 protects the SnO_2 based anode from irreversible reactions with the electrolyte, and buffers volumetric changes during lithiation/delithiation. The amorphous nature of the ALD HfO_2 films allows efficient diffusion of the lithium ions, even with thick HfO_2 passivation layers. Cyclic voltammetry (CV) results suggest that HfO_2 doesn't take part in electrochemical reaction, however, XPS analysis showed that an interaction took place between Hf and Sn, a process which apparently enhanced the lithiation reaction for the HfO_2 coated SnO_2 electrodes. Fig. 10 shows that schematic illustration of HfO_2 coating of SnO_2 nanospheres and corresponding electrochemical performance of bare SnO_2/rGO composite vs. HfO_2 passivated SnO_2/rGO composite electrodes [170].

Furthermore, our group has also studied the effect of HfO_2 passivation on MoO_3 nanorods [169], another anode material which experiences large volumetric changes during charge/discharge process. The improved cyclic performance at high current densities clearly indicates that HfO_2 combats the large volumetric changes and passivates the active material during charge/discharge process. In addition, the capacity retention mechanism was explained by ex situ HRTEM imaging and number of spectroscopic techniques, including XRD, Raman and XPS. The results showed that charge/discharge process distorts the crystal structure of MoO_3 and presence of HfO_2 layer serves as protective barrier at anode/electrolyte interface. Ex situ analysis clearly showed that HfO_2 assists in crystallinity retention and improves battery performance [169].

In addition to LIBs, we have also applied HfO_2 as passivation layer in Na ion batteries (NIBs) for MoS_2 nanosheet anodes [168]. In NIBs, after 50 charge/discharge cycles, bare MoS_2 and HfO_2 coated MoS_2 electrodes delivered the specific capacity of 435 and 636 mAh/g, respectively, at current density of 100 mA/g. These results imply that batteries using HfO_2 coated MoS_2 anodes retain 91% of the initial capacity; in contrast, bare MoS_2 anodes retain only 63%. Also, HfO_2 coated MoS_2 anodes show one of the highest reported capacity values for MoS_2 anodes. It is

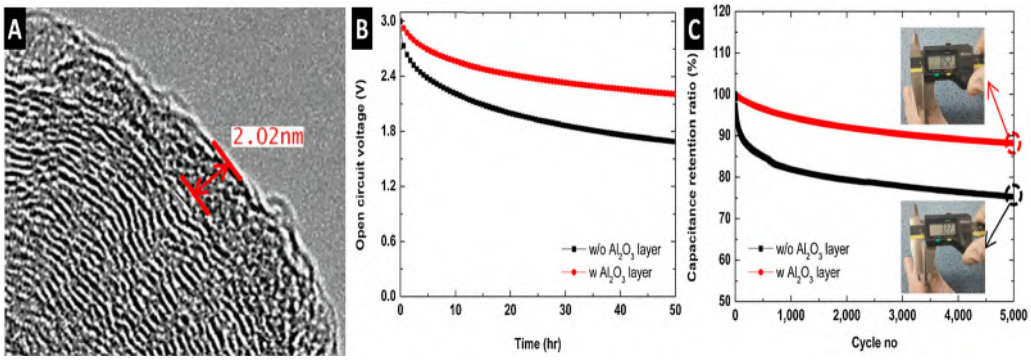

Figure 11 (A) HRTEM image of activated carbon with ALD Al_2O_3 layer. (B) Self-discharge of Carbon@Al_2O_3 electrode for 50 h. (C) Capacity retention during 5000 cycles at 70 °C, insets show the thickness after 5 K cycles.
Reproduced with permission from Hong et al., ACS Appl. Mater. Interfaces 7 (3) (2015) 1899—1906. Copyright 2015 American Chemical Society [87].

illustrated that HfO_2 acts as a passive protective layer at the anode/electrolyte interface and prevents structural degradation during charge/discharge process [168].

On NIBs front, TiO_2 has been also utilized as passive coating for MoS_2 nanofibers (NFs) [167]. The cyclic performance of these sulfides is extremely poor due to the continuous sulfur dissolution during charge/discharge process. The presence of TiO_2 protective layer improves the cyclic performance. After 30th cycle, the capacity retention of TiO_2 coated MoS_2 NFs is 64%, on the other hand the capacity retention for bare MoS_2 NFs is 30%. This result could be attributed to the significant reduction of the sulfur dissolution during the charge/discharge process due to TiO_2 layer [167]. Han et al. have investigated ALD Al_2O_3 passivated tin nanoparticles as anode material for NIBs by in situ TEM, which unveiled the dynamic mechanical protection of the ALD Al_2O_3 coating by coherently deforming with the Sn NPs under the huge volume changes during charge/discharge process [174]. The in situ techniques provide mechanistic insight and real rime evidence of the phenomenon of surface passivation.

ALD has also been used to deposit passive protective layers in electrochemical supercapacitors. While the carbonaceous materials show excellent charge-discharge stability in aqueous electrolyte, unfortunately, widely used activated carbon electrodes generally suffer from poor electrochemical stability above 2.5 V. One recent study showed that when activated carbon was conformally coated with two-nanometer thick Al_2O_3 dielectric layers by ALD deposition (Fig. 11a) 74% of initial voltage could be maintained 50 h after full charge, and 88% of capacitance was retained after 5000 cycles at 70 °C accelerated test, which correspond to 31 and 17% improvements from bare activated carbon, respectively (Fig. 11b and c) [87].

In another study, we demonstrated that unlike passive protective coatings, the electrochemically active oxide (RuO_2) could be used as buffer layer to enhance the cycling stability of conducting polymers (e.g. polyaniline) [89]. We developed a low-temperature ALD method to conformally deposit ultrathin RuO_2 film on polyaniline nanofiber arrays to form a stable supercapacitor electrode. The schematic illustration of PAni nanofiber growth on carbon cloth and ALD deposition of RuO_2 is shown in Fig. 12.

Because of the low ALD growth temperature (180 °C), the PAni polymer matrix remains intact (Fig. 13a). In addition, the chemical stability, high conductivity, and exceptional specific capacitance of RuO_2 was exploited to make polyaniline-RuO_2 core—shell structure that exhibits high specific capacitance (710 F/g at 5 mV/s) and power density (42.2 kW/kg) at an energy density of 10 Wh/kg (Fig. 13b—d). Furthermore, as shown in Fig. 13e, these core—shell electrodes exhibit remarkable capacitance retention of ca. 88% after 10,000 cycles, at very high current density of 20 A/g. This is a big improvement over pristine polyaniline-based pseudocapacitors (65% after 10,000 cycles), thanks to the ALD layer. We also found that the thickness of RuO_2 ALD layer showed a strong impact on the capacitive performance of the RuO_2/PAni electrode. An optimum thickness of RuO_2 was found to maximize capacitance (Fig. 13b). If the RuO_2 layer was too thick, the ion diffusion distance from electrolyte to PAni was increased, and the surface nanostructure of PAni surface (active sites) was eliminated, resulting in limited redox reactions, and hence lower performance devices. Fig. 13f shows the SEM image of RuO_2 coated PAni electrode after electrochemical testing, which shows that RuO_2 assists in structural preservation during charge/discharge process [89]. Without RuO_2, the PAni surface structure was destroyed (inset of Fig. 13f).

Electrolyte coatings

The prime requirement for solid-state electrolyte layer in supercapacitors and batteries is optimal thickness for electrical insulation and Li^+ ion conduction. The thickness ranges from 100 s nanometers to 10 s of microns in commonly used thin film batteries. However, electrolyte layer as thin as 10—20 nm has been also demonstrated and proved that thin inorganic electrolytes are beneficial in energy storage devices. As mentioned earlier, ALD provides excellent control over thickness and uniformity; therefore, ALD prepared electrolyte coatings can be tailored and applied in complex 3D structures. Table 4 summarizes the recent studies of ALD prepared solid state electrolytes in Li ion batteries. Aaltonen et al. has demonstrated the growth of thin films of lanthanum titanate (LT) and lithium lanthanum titanate (LLT

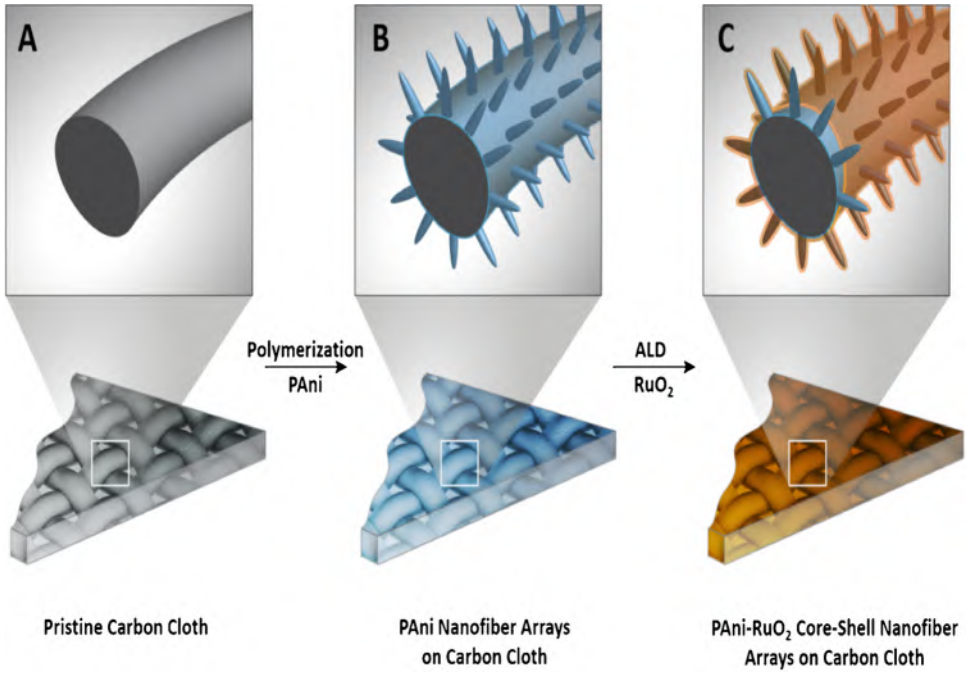

Figure 12 Schematic illustration of PAni/RuO_2 nanofibers core shells on carbon cloth as an electrode for symmetric pseudocapacitor: (A) pristine carbon fiber woven cloth; (B) PAni nanofiber arrays on carbon cloth by dilute polymerization of aniline; (C) PAni/RuO_2 core—shell nanofiber arrays on carbon cloth by further ALD growth of RuO_2 on the PAni NF arrays.
Reproduced with permission from Xia et al. Advanced Energy Materials, 5 (8) (2015). Copyright 2015 John Wiley & Sons, Inc. [89].

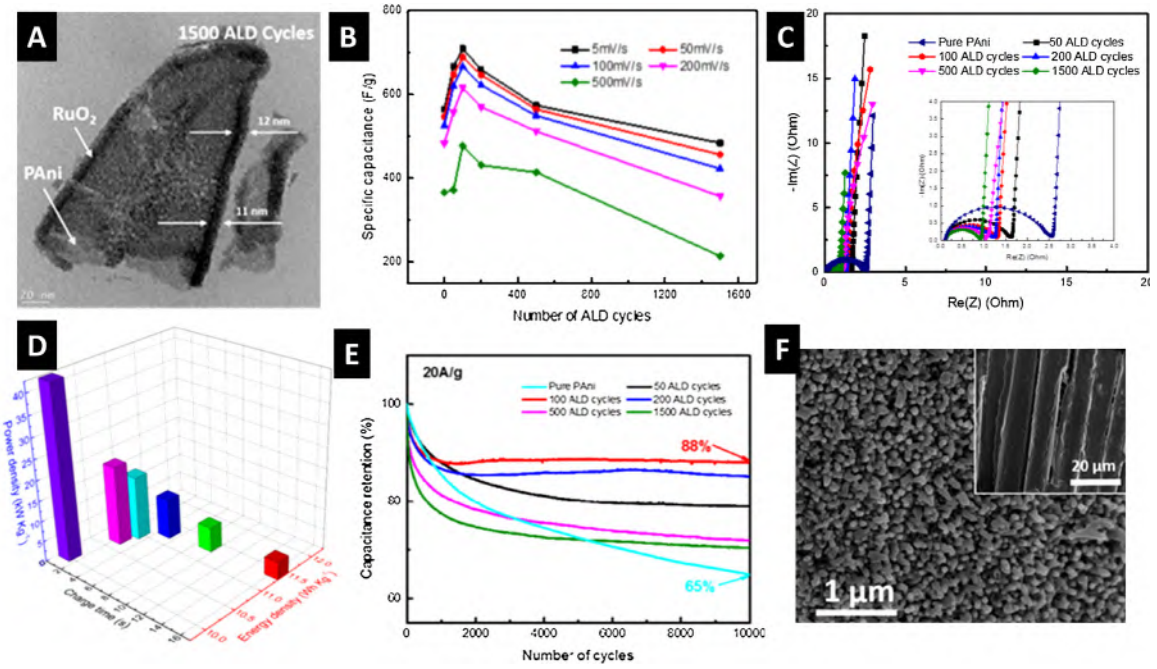

Figure 13 (A) Typical TEM image PAni/RuO_2 core—shell structure with 1500 ALD cycles, (B) summary of specific capacitance as function of number of ALD cycles, (C) Nyquist plots of all PAni/RuO_2 core—shell nanofiber based pseudocapacitors, (D) Ragone plot (energy density vs power density) of PAni-100ALD cycles of RuO_2 core—shell nanofiber based pseudocapacitors, (E) cycling stability of all PAni/RuO_2 core—shell nanofibers based pseudocapacitors and (F) FESEM of PAni-100 ALD cycles of RuO_2 core—shell nanofibers electrode and pure PAni electrode (inset) after 10,000 cycles. Note that the PAni structure is completely destroyed without RuO_2 surface coating after 10,000 cycles.
Reproduced with permission from Xia et al. Advanced Energy Materials 5 (8) (2015). Copyright 2015 John Wiley & Sons, Inc. [89].

Table 4 ALD fabricated electrolyte, separator and conductive coatings for Li ion batteries (LIBs).

Function	ALD materials	Commonly used configuration	Ref.
Electrolyte coating	$LiTaO_3$	LTO/LiNiCoMnO	[178]
	$Li_{5.1}TaO_z$	LTO/Si(100), LTO/AAO	[179]
	$Li_xAl_ySi_zO$	LASO/Si Nanowires	[180]
	Li_2O/Al_2O_3	Si(111) substrate	[176]
	Li_3PO_4	Si(111) substrate	[177]
Separator coating	Al_2O_3	Al_2O_3@Polypropylene, Polyethylene	[181,182]
	TiO_2	TiO_2@Polypropylene	[183]
Conductive coating	TiN	TiN@ $Li_4Ti_5O_{12}$	[184]

– $(Li,La)_xTi_yO_z$) by ALD [175]. The precursors used for the deposition of LT were $TiCl_4 + H_2O$ and $La_{(thd)3}$ (thd → 2,2,6,6-tetramethyl-3,5-heptanedione) + O_3. Lithium tert-butoxide (LiOtBu) and H_2O precursors were used to incorporate lithium for LLT deposition. Thin films of LLT have been reported to have significantly higher ionic conductivity than the commonly used solid state electrolyte—LiPON. However, the LLT layer is not stable in direct contact with most of the anode materials due to reduction of Ti^{4+} to Ti^{3+}. Therefore, a Li^+ ion conducting barrier layer should be deposited between the anode and the LLT electrolyte and LiO_2-Al_2O_3 served this purpose [176]. Lithium phosphate is another attractive electrolyte material in solid state LIBs because of its high ionic conductivity (≈6.6×10^{-8} S/cm at 25 °C for amorphous $Li_{2.7}PO_{3.9}$). Furthermore, Lithium phosphate can also be applied as interfacial layer between commonly used LIBs cathode – $LiCoO_2$ – and solid polymer electrolyte [177]. Hamalainen et al. has reported the ALD process for preparation of lithium phosphate (Li_3PO_4) thin films. A slightly crystalline Li_3PO_4 thin films were deposited in temperature range of 225 and 350 °C using trimethyl phosphate (TMOP) and either lithium hexamethyldisilazide or lithium tert-butoxide [177].

Moreover, ALD prepared thin films of lithium aluminosilicate ($Li_xAl_ySi_zO$) as solid state electrolyte has also been demonstrated for Li ion batteries. $Li_xAl_ySi_zO$ was deposited at 290 °C using LiOH, Al_2O_3 and SiO_2 precursors [180]. The as-deposited amorphous ALD electrolyte layers are found to be conformal and free of pinholes over Si nanowires. Other ALD prepared electrolyte layers include $LiAlO_x$, Li_3N, $LiNbO_3$ and $LiTaO_3$ and it is believed that because of its unique coating mechanism, ALD will play vital role in development of electrolytes for solid state mircobatteries. In addition, these electrolyte films have potential to perform better than the metal oxide passive coatings discussed in the passive coatings section [178]. Though the solid state electrolyte and metal oxide films have not been compared in terms of their protective effect, Fig. 14 illustrates the concept of Li ion conducting films and metal oxide films on electrode/electrolyte interface. Current research is mainly focused on development of ALD processes for solid state electrolyte with high ionic conductivities.

Sacrificial coatings

As previously discussed, the ALD method enables deposition of uniform and conformal ultrathin films on very high-aspect-ratio substrates or nanoparticles. Hence, some ALD materials (e.g. Al_2O_3) were further investigated as sacrificial coating to obtain various unique nanostructures such as nanogap and porous carbon coating [90–93]. Fan's group reported the first successful preparation of rough carbon nanoflakes on metal oxide nanostructures by combining ALD and glucose carbonization which is illustrated in Fig. 15a [93]. More specifically, a unique hierarchical 3D $Co_2(OH)_2CO_3$ nanowire arrays were synthesized using a facile hydrothermal route. Next, a sacrificial amorphous Al_2O_3 layer was controllably grown on the nanowire surface by ALD. Afterwards, $Co_2(OH)_2CO_3$@Al_2O_3 was immersed into a glucose solution to transform the outer Al_2O_3 shell into a Al_2O_3-glucose composite. In the next annealing process, the glucose carbonizes and also causes a simultaneous fragmentation of the Al_2O_3. The fragmented Al_2O_3 remains attached to the carbon during the formation of an elongated structure. In the meantime, the $Co_2(OH)_2CO_3$ will decomposed to CoO. Finally, the CoO@carbon flakes core–shell structure (Fig. 15b) was formed by post-etching of Al_2O_3 in

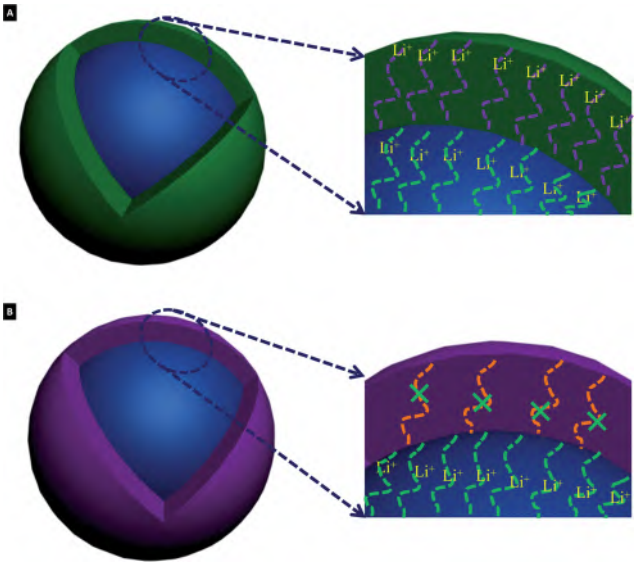

Figure 14 Schematic illustration of the difference between (a) solid state electrolyte coatings and (b) metal oxide coatings. The former provides higher lithium ion conductivity than the latter.
Reproduced from [178] with permission from The Royal Society of Chemistry.

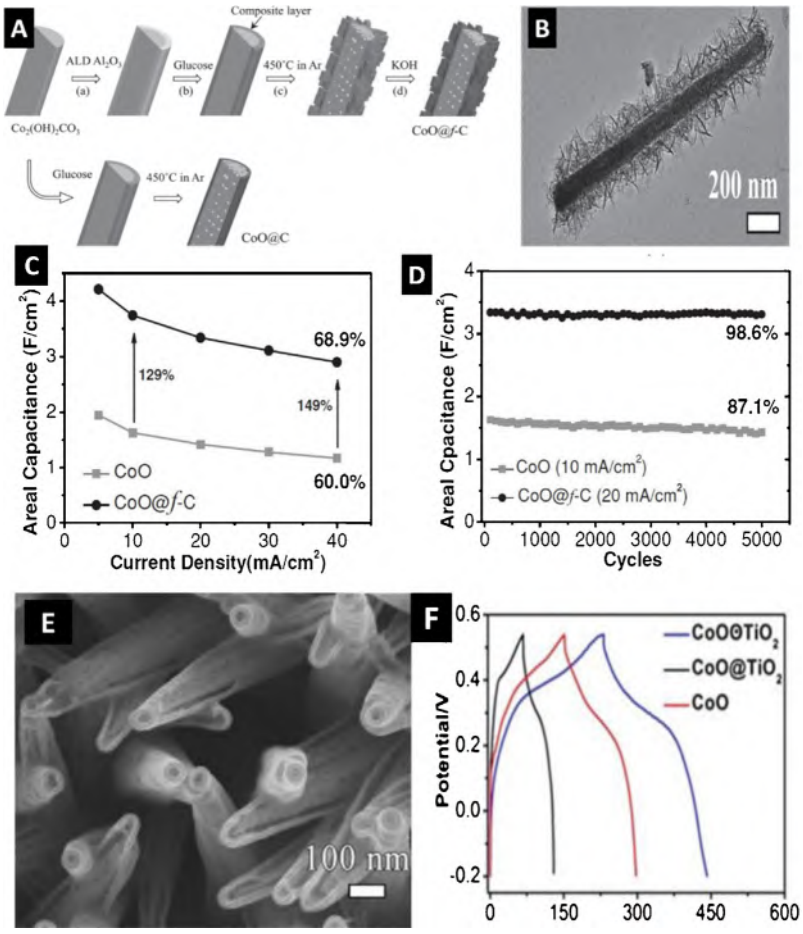

Figure 15 (A) Schematics of the fabrication processes of rough carbon flakes and dense carbon film coating on CoO nanowire, (B) representative SEM image of carbon flakes covered individual CoO nanowire, (C and D) supercapacitor performance of CoO and carbon flakes decorated CoO nanowire arrays, (E) typical SEM image of hollow CoO@TiO_2 core—shell nanostructure (''wire in tube'' structure) and (F) Charge—discharge curve of the three structures (CoO, CoO@TiO_2 and hollow CoO@TiO_2) at the same current density of 10 mA/cm^2. Panels (A—D) are reproduced with permission from Guan et al. Small 10 (2) (2014) 300—307. Copyright 2014 John Wiley & Sons, Inc. [93]. Panels (E—F) are reproduced from [90] with permission from The Royal Society of Chemistry.

KOH solution. As summarized in Fig. 15c and d, when tested as supercapacitor electrode, the hierarchical CoO@carbon nanostructured flakes exhibit much higher specific capacitance (930.9 F/g) compared to the pristine CoO (452.8 F/g) or the carbon coating without ALD (476.5 F/g). Moreover, at a charge/discharge current density of 10 mA/cm^2, the capacitance retention of CoO after 5000 cycles was 87.1%. In contrast, the CoO@carbon flakes retained 98% of their capacitance after 5000 cycles even at a higher current density of 20 mA/cm^2. The authors pointed out that the ALD Al_2O_3 layer is critical to synthesizing the rough and porous outer carbon shell, and is the main factor to determine the thickness of the carbon shell. Based on the control experiments, the directly coated dense carbon film on CoO nanowire could not enhance the capacitive performance of CoO. The enhancement of the electrochemical properties of CoO@carbon flakes can be attributed to increased specific surface areas and electric conductivity due to the roughness of carbon flake coating [93]. Similar concepts were later extended to $Ni_xCo_{1-x}O$ and Co_3O_4 system by other researchers [92,93] which confirmed the importance of the sacrificial ALD layer. As another interesting example, Guan et al. showed that a thin sacrificial Al_2O_3 layer (deposited by ALD and removed eventually) could be utilized to create nanogap between the CoO core and the TiO_2 shell [90]. Fig. 15e reveals the typical SEM image of as-prepared hollow CoO@TiO_2 core—shell nanostructure. In supercapacitor applications, an evident difference between the solid core—shell (CoO@TiO_2) nanostructure and hollow ones (CoO@nanogap@TiO_2) can be found (Fig. 15f); for example, the hollow structure shows higher capacitance, better rate performance and cycling stability compared to the solid wires. The electrochemical properties are also superior compared to the bare nanorods without the outer TiO_2 shell. It was proposed that the nanogap provides an increased reaction area and facilitates the electrolyte contact with the active material. In addition, the outer tube layer preserves the structural integrity after long-time cycling. As a result, such a hollow core—shell nanostructures were more efficient in supercapacitor applications compared with their solid core—shell, bare core counterparts.

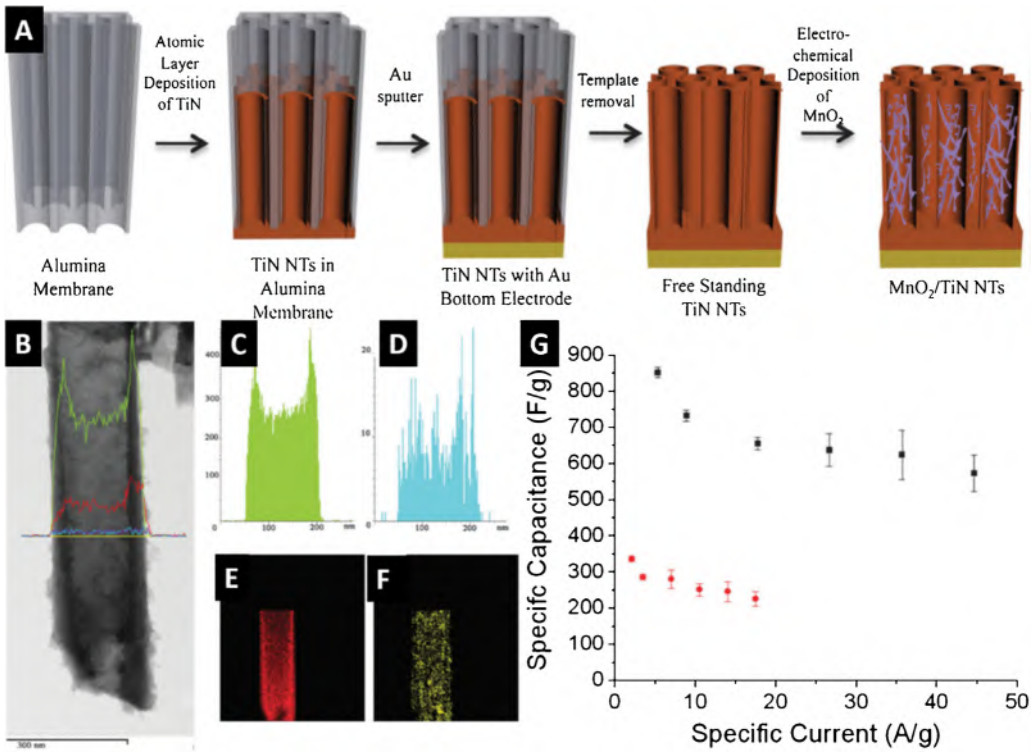

Figure 16 (A) Schematics of the fabrication processes of MnO_2/TiN naotubes, (B) TEM image of a single MnO_2/TiN nanotube, EDS line scan of (C) titanium (D) manganese and EDS mapping of (E) titanium and (F) manganese and (G) Supercapacitor performance of CoO and carbon flakes decorated CoO nanowire arrays.
Reproduced from [96] with permission from The Royal Society of Chemistry.

Conductive coatings

Highly conductive 3D scaffolds are normally employed to grow electroactive materials in energy storage applications. Recently, ALD was employed to fabricate self-supporting conductive 3D structures using porous anodic aluminum oxide (AAO) as nano-template [94—96]. TiN, for instance, was ALD deposited into a porous AAO template to prepare TiN nanotube arrays [96]. After template removal, the inner and outer surfaces of the TiN nanotubes are exposed for electrochemical deposition of manganese oxide. The whole synthesis process has been clearly described in Fig. 16a. Furthermore, a representative TEM image and corresponding EDS line scan reveal the successful formation of TiN nanotube and TiN@MnO_2 heterostructure (Fig. 16b—f). Due to the close proximity of MnO_2 with the highly conductive TiN as well as the overall high surface area, the nanotubes show very high specific capacitance (662 F/g reported at 45 A/g) as a supercapacitor electrode material. The highly conductive and mechanically stable TiN greatly enhances the flow of electrons to the MnO_2 material, while the high aspect ratio nanostructure of TiN creates a large surface area for short diffusion paths for cations thus improving high power. Otherwise, SnO_2 [94] and Pt [95] were also chosen as conductive coating materials to form a tube-like 3D matrix to support the MnO_2 for supercapacitor applications. The resultant performance showed that combining the favorable structural and electrical properties of MnO_2 with conductive support into one system allows for a promising electrode material for supercapacitors.

Separator coatings

Except in solid state energy storage devices, various liquid electrolytes are used for ionic movement during charge/discharge process. To fully utilize the available electrode surface area, the access of liquid electrolyte to the surface of electrode material should be as high as possible. Apart from an open electrode structure, two important factors come from separators: porosity and wettability. The wettability of conventional polymer separators can be improved by various surface modification techniques such as polymer coatings and a polydopamine treatment. Due to the unique deposition mechanism of ALD, it has been utilized for surface modification of polymeric substrate. Jung et al. has reported that a thin layer of ALD deposited Al_2O_3 significantly suppress the thermal shrinkage, which can be beneficial in terms of device safety [181]. Furthermore, the wettability of Al_2O_3 coated polymeric membrane is improved, when pure propylene carbonate (PC) solvent is used [181]. Woo et al. has first utilized ALD to modify the surface of polymeric separator and, later, processed it into an ion-exchangeable functional separator [182]. The have used this separator in a full cell of Li ion battery where $LiMn_2O_4$ was used as cathode and graphite was used as anode. Fig. 17a presents the schematic diagram for the fabrication of ion-exchangeable functional separator, while Fig. 17b shows the schematic illustration for the principle of an ion-exchangeable separator. Briefly, Na^+ ions from the functional groups of the separator and dissolved Mn^{2+} ions exchange during electrochemical process which results in entrapment

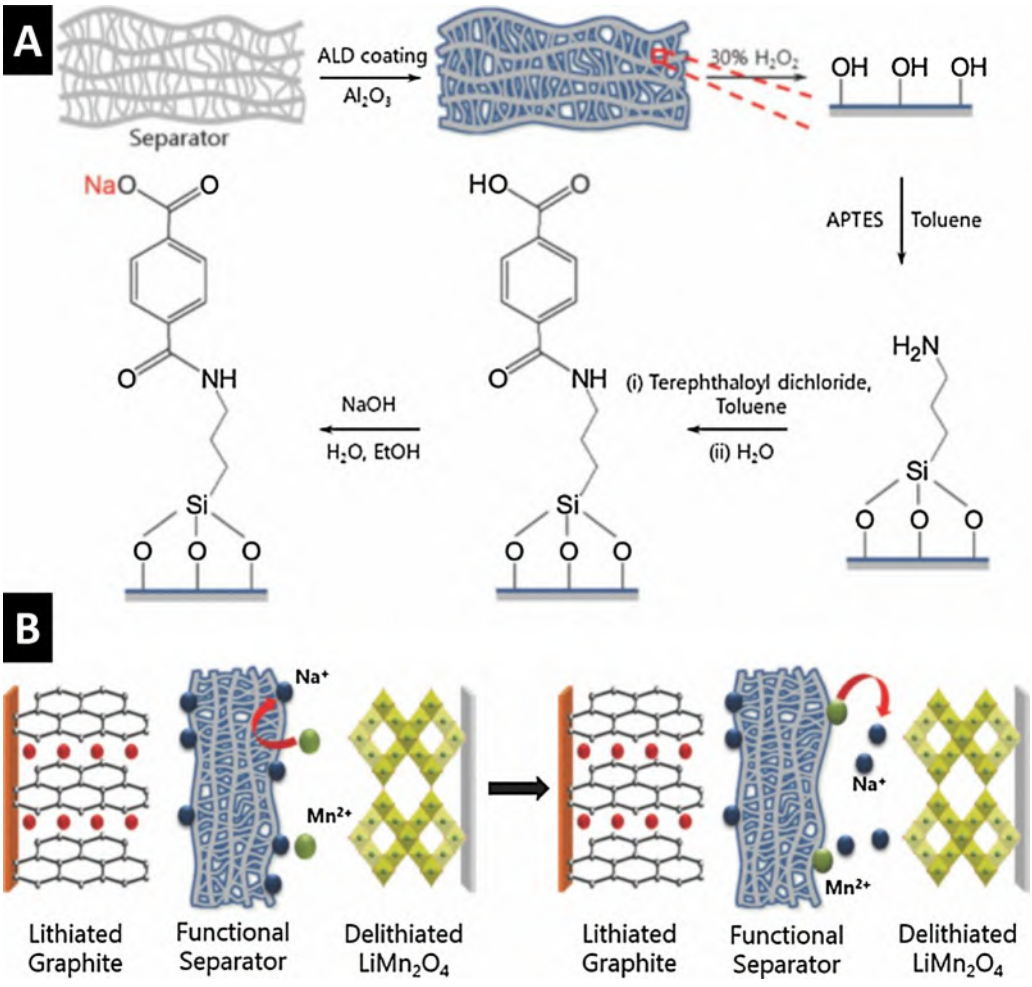

Figure 17 (A) Schematic diagram for the synthesis of an ion exchangeable separator and (B) mechanism of how this separator inhibits Mn-assisted degradation.
Reproduced from Ref. [182] with permission from the Electrochemical Society.

of dissolved Mn^{2+} ions and inhibits self-discharge. That's why the overall cyclic performance is improved. Another group has deposited ultrathin layer of TiO_2 by ALD on polypropylene [183]. They have found that plasma activation plays key role in final performance of separators. Plasma activation makes bare separators ready for ALD process and an ultrathin, yet effective, layer of TiO_2 can be conformally deposited with low number of cycles. The ALD TiO_2 layer effectively suppresses the thermal shrinkage of the separators and improves the wettability [183]. Due to the conformal nature of the ALD process, thin coatings do not alter the pore structure, thus electrochemical performance is not compromised.

Conclusions & perspective

In summary, we have reviewed the literature on the use of atomic layer deposition to improve the performance of rechargeable batteries and supercapacitors. The ALD coatings have been used to perform various functions in energy storage devices, which can be broadly classified into: active coatings, passive coatings, conductive coatings, separator coatings, electrolyte coatings and sacrificial coatings. In some cases, the coated layer could provide more than one function in the same device. Moreover, ALD coating of same material can perform differently depending upon coating thickness, substrate and operating conditions. For instance, thin layer of TiO_2 has been reported as passive layer [167], while a relatively thicker layer becomes active anode materials for LIBs [45]. Similarly, V_2O_5 has been reported as cathode electrode [36] when deposited on current collector but deposition of amorphous V_2O_5 on graphene sheets behaves as passive layer [185]. The ALD method clearly offers several key advantages which have been beneficial in developing of our understanding of various phenomena in electrochemical energy storage devices. For instance, the conformality and precise thickness control of the ALD method has allowed researchers to carry out studies nearly independent of the shape of the nanomaterial or the current collector. This can be clearly seen in experiments where three dimensional current collectors (e.g., Ni foams) were easily coated by atomic layer deposition. This type of structure has an advantage, particularly in case of supercapacitors, to decouple electrolyte diffusion from surface reactions, which has helped to more effectively

evaluate material performance. We showed that nanomaterials with a broad spectrum of dimensionality can be coated by ALD: one dimensional (e.g., nanowires), two dimensional (2D) materials (e.g., transition metal chalcogenides), and three dimensional materials (e.g., graphene and chalcogenide foams). In addition, the ALD layer could be deposited on many types of anode and cathode materials because of its low deposition temperature, which is well below 200 °C for most materials. Another clear advantage in the reported studies is that the ALD-coated layers remain uniform, even when significantly thin, which means that researchers can change the surface chemistry or reduce the SEI layer formation without significantly hindering diffusion of the mobile ions such as Li and Na ions.

Going forward, there are a number of issues that need further studies in this important field of research. This should include the development of ALD processes for additional battery materials to leverage emerging new materials and 3D architectures. This should, for example, include development of processes for 2D materials (such as sulfides and selenides of transition elements and MXenes) and their nanocomposites. More detailed studies on the diffusion of Na and Li ion through the coated layers by experimental and theoretical simulation (e.g., ab-initio molecular dynamics calculations under electric fields) is needed. For example, in our own studies, we have seen that the critical thickness at which HfO_2 ALD coatings blocks Li^+ ion diffusion toward the active material is higher than other ALD oxides such as Al_2O_3. If one can predict diffusion coefficients of mobile ions (Li, Na, or even Mg) in various ALD layers, such simulations could provide useful information to experimentalists. Another important area of research is in situ studies on the electrode material with and without ALD coatings. Although nearly 150 reports have been published on ALD coatings on battery electrodes, the truth is that the mechanistic understanding of how these oxides can slow down battery degradation is not always clear. Studies using in situ X-ray diffraction, Raman spectroscopy, TEM and XPS can provide mechanistic insight and should be expanded. Another topic of interest has to do with the growth conditions of coated materials. The reactant gas (e.g. water vs ozone in case of oxides) is known to affect the properties of the grown ALD layer. Furthermore, plasma enhanced ALD growth of ALD layers can improve their quality and density, so more studies are needed to fully explore this feature. This is because often the plasma can remove the grown ALD films of hydrocarbons and halogens that are left over from the growth process. The role of these remnants in grown film may actually be important for the performance of the ALD coating. Hence the precursor chemistry (organometallic vs halide) should also be explored. The growth temperature of the ALD layer can also have a big impact on ALD coating performance and should be explored in more detail. Like reacting agents, the temperature of ALD growth could also affect film density, purity, and microstructure, which can intern determine its efficacy in electrochemical energy storage devices. Another issue is the role of fluorine in the electrolyte, some ALD layers may be more readily attached by fluorine than others, which comprises the integrity of the layer. This effect needs to be further elaborated to test any correlation between the ALD effect on device stability and its propensity to be attacked by fluorine or fluorine-containing species. Finally, the issue of cost of the ALD process for electrochemical energy storage applications must be addressed. The ALD process is certainly more costly than chemical processes such as sol–gel for electrode coating applications. However, ALD system cost has to be reconciled with the benefit, impact on device performance, and process yields.

Acknowledgments

This research was supported by King Abdullah University of Science & Technology (KAUST). The authors wish to thank Mr. Hyunho Kim for his help with the technical illustrations.

References

[1] J.B. Goodenough, K.-S. Park, J. Am. Chem. Soc. 135 (2013) 1167–1176.
[2] S. Chu, A. Majumdar, Nature 488 (2012) 294–303.
[3] G.L. Soloveichik, Annu. Rev. Chem. Biomol. Eng. 2 (2011) 503–527.
[4] M.M. Thackeray, C. Wolverton, E.D. Isaacs, Energy Environ. Sci. 5 (2012) 7854–7863.
[5] A. Vu, Y. Qian, A. Stein, Adv. Energy Mater. 2 (2012) 1056–1085.
[6] J. Cabana, L. Monconduit, D. Larcher, M.R. Palacín, Adv. Mater. 22 (2010) E170–E192.
[7] P.G. Bruce, S.A. Freunberger, L.J. Hardwick, J.-M. Tarascon, Nat. Mater. 11 (2012) 19–29.
[8] Z. Peng, S.A. Freunberger, Y. Chen, P.G. Bruce, Science 337 (2012) 563–566.
[9] X. Ji, K.T. Lee, L.F. Nazar, Nat. Mater. 8 (2009) 500–506.
[10] M.M. Ottakam Thotiyl, S.A. Freunberger, Z. Peng, Y. Chen, Z. Liu, P.G. Bruce, Nat. Mater. 12 (2013) 1050–1056.
[11] M. Dubois, D. Billaud, J. Solid State Chem. 127 (1996) 123–125.
[12] J. Barker, R.K.B. Gover, P. Burns, A.J. Bryan, Electrochem. Solid-State Lett. 9 (2006) A190–A192.
[13] P. Simon, Y. Gogotsi, B. Dunn, Science 343 (2014) 1210–1211.
[14] L. Zhang, X. Zhang, Z. Wang, J. Xu, D. Xu, L. Wang, Chem. Commun. 48 (2012) 7598–7600.
[15] H. Jiang, J. Ma, C. Li, Adv. Mater. 24 (2012) 4197–4202.
[16] W. Wei, X. Cui, W. Chen, D.G. Ivey, Chem. Soc. Rev. 40 (2011) 1697–1721.
[17] N.-S. Choi, Z. Chen, S.A. Freunberger, X. Ji, Y.-K. Sun, K. Amine, et al., Angew. Chem. Int. Ed. 51 (2012) 9994–10024.
[18] A. Manthiram, J. Phys. Chem. Lett. 2 (2011) 176–184.
[19] P.G. Bruce, B. Scrosati, J.-M. Tarascon, Angew. Chem. Int. Ed. 47 (2008) 2930–2946.
[20] G. Jeong, J.-H. Kim, Y.-U. Kim, Y.-J. Kim, J. Mater. Chem. 22 (2012) 7999–8004.
[21] J. Xiao, W. Xu, D. Wang, D. Choi, W. Wang, X. Li, et al., J. Electrochem. Soc. 157 (2010) A1047–A1051.
[22] T. Suntola, J. Antson, US Patent 4058430 A, 1977.
[23] T. Suntola, Mater. Sci. Eng. Rep. 4 (1989) 261–312.
[24] H. Kim, J. Vac. Sci. Technol. B 21 (2003) 2231–2261.
[25] A.C. Dillon, A.W. Ott, J.D. Way, S.M. George, Surf. Sci. 322 (1995) 230–242.
[26] J.E. Crowell, J. Vac. Sci. Technol. A 21 (2003) S88–S95.
[27] R.L. Puurunen, J. Appl. Phys. 97 (2005) 121301–121352.
[28] A. Paranjpe, S. Gopinath, T. Omstead, R. Bubber, et al., J. Electrochem. Soc. 148 (2001) G465–G471.
[29] J.C. Badot, S. Ribes, E.B. Yousfi, V. Vivier, J.P. Pereira-Ramos, N. Baffier, et al., Electrochem. Solid-State Lett. 3 (2000) 485–488.

[30] R. Baddour-Hadjean, V. Golabkan, J.P. Pereira-Ramos, A. Mantoux, D. Lincot, J. Raman Spectrosc. 33 (2002) 631–638.
[31] F. Lantelme, A. Mantoux, H. Groult, D. Lincot, Electrochim. Acta 47 (2002) 3927–3938.
[32] F. Lantelme, A. Mantoux, H. Groult, D. Lincot, J. Electrochem. Soc. 150 (2003) A1202–A1208.
[33] J.C. Badot, A. Mantoux, N. Baffier, O. Dubrunfaut, D. Lincot, J. Phys. Chem. Solids 67 (2006) 1270–1274.
[34] H. Groult, K. Le Van, A. Mantoux, L. Perrigaud, F. Lantelme, R. Lindstrom, et al., J. Power Sources 160 (2006) 592–601.
[35] X. Chen, E. Pomerantseva, P. Banerjee, K. Gregorczyk, R. Ghodssi, G. Rubloff, Chem. Mater. 24 (2012) 1255–1261.
[36] X. Chen, H. Zhu, Y.C. Chen, Y. Shang, A. Cao, L. Hu, et al., ACS Nano 6 (2012) 7948–7955.
[37] X. Chen, E. Pomerantseva, K. Gregorczyk, R. Ghodssi, G. Rubloff, RSC Adv. 3 (2013) 4294–4302.
[38] E. Ostreng, K.B. Gandrud, Y. Hu, O. Nilsen, H. Fjellvag, J. Mater. Chem. A 2 (2014) 15044–15051.
[39] M.E. Donders, H.C.M. Knoops, W.M.M. Kessels, P.H.L. Notten, Atomic Layer Depos. Appl. 7 (41) (2011) 321–330.
[40] J. Liu, B. Xiao, M.N. Banis, R. Li, T.-K. Sham, X. Sun, Electrochim. Acta 162 (2015) 275–281.
[41] L. Jian, M.N. Banis, S. Qian, A. Lushington, L. Ruying, S. Tsun-Kong, et al., Adv. Mater. 26 (2014) 6472–6477.
[42] Y. Lei, J. Lu, X. Luo, T. Wu, P. Du, X. Zhang, et al., Nano Lett. 13 (2013) 4182–4189.
[43] X. Meng, D.J. Comstock, T.T. Fister, J.W. Elam, ACS Nano 8 (2014) 10963–10972.
[44] J.M. Haag, G. Pattanaik, M.F. Durstock, Adv. Mater. 25 (2013) 3238–3243.
[45] S.-W. Kim, T.H. Han, J. Kim, H. Gwon, H.-S. Moon, S.-W. Kang, et al., ACS Nano 3 (2009) 1085–1090.
[46] L. Xifei, M. Xiangbo, L. Jian, G. Dongsheng, Z. Yong, M.N. Banis, et al., Adv. Funct. Mater. 22 (2012) 1647–1654.
[47] W. Wang, M. Tian, A. Abdulagatov, S.M. George, Y.-C. Lee, R. Yang, Nano Lett. 12 (2012) 655–660.
[48] X. Meng, J.A. Libera, T.T. Fister, H. Zhou, J.K. Hedlund, P. Fenter, et al., Chem. Mater. 26 (2014) 1029–1039.
[49] M. Xiangbo, H. Kai, S. Dong, Z. Xiaofeng, S. Chengjun, R. Yang, et al., Adv. Funct. Mater. 24 (2014) 5435–5442.
[50] D.K. Nandi, U.K. Sen, D. Choudhury, S. Mitra, S.K. Sarkar, ACS Appl. Mater. Interfaces 6 (2014) 6606–6615.
[51] C. Bae, Y. Yoon, W.-S. Yoon, J. Moon, J. Kim, H. Shin, ACS Appl. Mater. Interfaces 2 (2010) 1581–1587.
[52] K. Gerasopoulos, X. Chen, J. Culver, C. Wang, R. Ghodssi, Chem. Commun. 46 (2010) 7349–7351.
[53] S.K. Panda, Y. Yoon, H.S. Jung, W.-S. Yoon, H. Shin, J. Power Sources 204 (2012) 162–167.
[54] C. Ban, M. Xie, X. Sun, J.J. Travis, G. Wang, H. Sun, et al., Nanotechnology 24 (2013) 424002–424007.
[55] J.-H. Jeun, K.-Y. Park, D.-H. Kim, W.-S. Kim, H.-C. Kim, B.-S. Lee, et al., Nanoscale 5 (2013) 8480–8483.
[56] R. Li, Z. Xie, H. Lu, D.W. Zhang, A. Yu, Int. J. Electrochem. Sci. 8 (2013) 11118–11124.
[57] J. Luo, X. Xia, Y. Luo, C. Guan, J. Liu, X. Qi, et al., Adv. Energy Mater. 3 (2013) 737–743.
[58] S. Moitzheim, C.S. Nimisha, S. Deng, D.J. Cott, C. Detavernier, P.M. Vereecken, Nanotechnology 25 (2014) 504008–504016.
[59] C. Zhu, X. Xia, J. Liu, Z. Fan, D. Chao, H. Zhang, et al., Nano Energy 4 (2014) 105–112.
[60] Z. Haifeng, R. Weina, C. Chuanwei, Nanotechnology 26 (2015) 274002–274009.
[61] M. Kim, J. Lee, S. Lee, S. Seo, C. Bae, H. Shin, ChemSusChem 8 (2015) 2363–2371.
[62] M. Li, X. Li, W. Li, X. Meng, Y. Yu, X. Sun, Electrochem. Commun. 57 (2015) 43–47.
[63] M. Tian, W. Wang, Y. Liu, K.L. Jungjohann, C.T. Harris, Y.-C. Lee, et al., Nano Energy 11 (2015) 500–509.
[64] J. Ye, A.C. Baumgaertel, Y.M. Wang, J. Biener, M.M. Biener, ACS Nano 9 (2015) 2194–2202.
[65] K.E. Gregorczyk, A.C. Kozen, X. Chen, M.A. Schroeder, M. Noked, A. Cao, et al., ACS Nano 9 (2015) 464–473.
[66] V. Aravindan, K.B. Jinesh, R.R. Prabhakar, V.S. Kale, S. Madhavi, Nano Energy 2 (2013) 720–725.
[67] D.K. Nandi, U.K. Sen, S. Sinha, A. Dhara, S. Mitra, S.K. Sarkar, Phys. Chem. Chem. Phys. 17 (2015) 17445–17453.
[68] M. Xiangbo, S.C. Riha, J.A. Libera, W. Qingliu, W. Hsien-Hau, A.B.F. Martinson, et al., J. Power Sources 280 (2015) 621–629.
[69] M.E. Donders, H.C.M. Knoops, W.M.M. Kessels, P.H.L. Notten, J. Power Sources 203 (2012) 72–77.
[70] S. Xiang, Z. Changgong, X. Ming, S. Hongtao, H. Tao, L. Fengyuan, et al., J. Mater. Chem. A 2 (2014) 7319–7326.
[71] C. Zhu, P. Yang, D. Chao, X. Wang, X. Zhang, S. Chen, et al., Advanced materials (Deerfield Beach. Fla.) 27 (2015) 4566–4571.
[72] K. Grigoras, J. Keskinen, L. Grönberg, J. Ahopelto, M. Prunnila, J. Phys.: Conf. Ser. 557 (2014) 012058.
[73] F. Grote, H. Zhao, Y. Lei, J. Mater. Chem. A 3 (2015) 3465–3470.
[74] R. Warren, F. Sammoura, F. Tounsi, M. Sanghadasa, L. Lin, J. Mater. Chem. A 3 (2015) 15568–15575.
[75] R.A. Fisher, M.R. Watt, R. Konjeti, W.J. Ready, ECS J. Solid State Sci. Technol. 4 (2015) M1–M5.
[76] X. Sun, M. Xie, J.J. Travis, G. Wang, H. Sun, J. Lian, et al., J. Phys. Chem. C 117 (2013) 22497–22508.
[77] X. Sun, M. Xie, G. Wang, H. Sun, A.S. Cavanagh, J.J. Travis, et al., J. Electrochem. Soc. 159 (2012) A364–A369.
[78] S. Boukhalfa, K. Evanoff, G. Yushin, Energy Environ. Sci. 5 (2012) 6872–6879.
[79] J. Benson, S. Boukhalfa, A. Magasinski, A. Kvit, G. Yushin, ACS Nano 6 (2012) 118–125.
[80] C. Guan, Y. Wang, Y. Hu, J. Liu, K.H. Ho, W. Zhao, et al., J. Mater. Chem. A 3 (2015) 23283–23288.
[81] C. Caiying, C. Chaoqiu, H. Peipei, D. Feifei, Z. Shichao, L. Ping, et al., Nanotechnology 25 (2014) 504001–504009.
[82] G. Cao, Q. Xu, W. Xinghui, C. Yanqiang, Z. Qing, L. Aidong, et al., Nanotechnology 26 (2015) 094001–094009.
[83] H. Li, Y. Gao, Y. Shao, Y. Su, X. Wang, Nano Lett. 15 (2015) 6689–6695.
[84] F. Yang, L. Zhang, A. Zuzuarregui, K. Gregorczyk, L. Li, M. Beltrán, et al., ACS Appl. Mater. Interfaces 7 (2015) 20513–20519.
[85] M. Gnerlich, E. Pomerantseva, K. Gregorczyk, D. Ketchum, G. Rubloff, R. Ghodssi, J. Micromech. Microeng. 23 (2013) 114014–114020.
[86] C. Guan, J. Liu, Y. Wang, L. Mao, Z. Fan, Z. Shen, et al., ACS Nano 9 (2015) 5198–5207.
[87] K. Hong, M. Cho, S.O. Kim, ACS Appl. Mater. Interfaces 7 (2015) 1899–1906.
[88] Z. Gui, H. Zhu, E. Gillette, X. Han, G.W. Rubloff, L. Hu, et al., ACS Nano 7 (2013) 6037–6046.
[89] X. Chuan, C. Wei, W. Xianbin, M.N. Hedhili, W. Nini, H.N. Alshareef, Adv. Energy Mater. 5 (2015) 1401805–1401813.
[90] C. Guan, X. Xia, N. Meng, Z. Zeng, X. Cao, C. Soci, et al., Energy Environ. Sci. 5 (2012) 9085–9090.
[91] G. Cao, W. Yadong, Z. Margit, W. John, F. Hong Jin, Nanotechnology 26 (2015) 014001–014009.
[92] R. Zhang, J. Liu, H. Guo, X. Tong, Mater. Lett. 134 (2014) 190–193.
[93] C. Guan, Z. Zeng, X. Li, X. Cao, Y. Fan, X. Xia, et al., Small 10 (2014) 300–307.
[94] F. Grote, L. Wen, Y. Lei, J. Power Sources 256 (2014) 37–42.
[95] L. Wen, Y. Mi, C. Wang, Y. Fang, F. Grote, H. Zhao, et al., Small 10 (2014) 3162–3168.
[96] S.A. Sherrill, J. Duay, Z. Gui, P. Banerjee, G.W. Rubloff, S.B. Lee, Phys. Chem. Chem. Phys. 13 (2011) 15221–15226.

Please cite this article in press as: B. Ahmed, et al., Nano Today (2016), http://dx.doi.org/10.1016/j.nantod.2016.04.004

[97] L. Jian, S. Xueliang, Nanotechnology 26 (2015) 024001—024014.
[98] X. Wang, G. Yushin, Energy Environ. Sci. 8 (2015) 1889—1904.
[99] Y.S. Jung, A.S. Cavanagh, L.A. Riley, S.-H. Kang, A.C. Dillon, M.D. Groner, et al., Adv. Mater. 22 (2010) 2172—2176.
[100] J.-T. Lee, F.-M. Wang, C.-S. Cheng, C.-C. Li, C.-H. Lin, Electrochim. Acta 55 (2010) 4002—4006.
[101] J. Yoon Seok, A.S. Cavanagh, A.C. Dillon, M.D. Groner, S.M. George, L. Se-Hee, J. Electrochem. Soc. 157 (2010) A75—A81.
[102] Y.S. Jung, A.S. Cavanagh, Y. Yan, S.M. George, A. Manthiram, J. Electrochem. Soc. 158 (2011) A1298—A1302.
[103] L.A. Riley, S. Van Ana, A.S. Cavanagh, Y. Yan, S.M. George, P. Liu, et al., J. Power Sources 196 (2011) 3317—3324.
[104] I.D. Scott, Y.S. Jung, A.S. Cavanagh, Y. An, A.C. Dillon, S.M. George, et al., Nano Lett. 11 (2011) 414—418.
[105] H.-M. Cheng, F.-M. Wang, J.P. Chu, R. Santhanam, J. Rick, S.-C. Lo, J. Phys. Chem. C 116 (2012) 7629—7637.
[106] D. Liu, Y. Liu, S.L. Candelaria, G. Cao, J. Liu, Y.-H. Jeong, J. Vac. Sci. Technol. A 30 (2012), 01A123—01A128.
[107] X. Luan, D. Guan, Y. Wang, J. Nanosci. Nanotechnol. 12 (2012) 7113—7120.
[108] M. Bettge, Y. Li, B. Sankaran, N.D. Rago, T. Spila, R.T. Haasch, et al., J. Power Sources 233 (2013) 346—357.
[109] D. Guan, Y. Wang, Ionics 19 (2013) 1—8.
[110] X. Xiao, D. Ahn, Z. Liu, J.-H. Kim, P. Lu, Electrochem. Commun. 32 (2013) 31—34.
[111] J. Yoon Seok, L. Peng, A.S. Cavanagh, B. Chunmei, K. Gi-Heon, L. Se-Hee, et al., Adv. Energy Mater. 3 (2013) 213—219.
[112] X. Zhang, I. Belharouak, L. Li, Y. Lei, J.W. Elam, A. Nie, et al., Adv. Energy Mater. 3 (2013) 1299—1307.
[113] J. Zhao, Y. Wang, J. Solid State Electrochem. 17 (2013) 1049—1058.
[114] X. Fang, M. Ge, J. Rong, Y. Che, N. Aroonyadet, X. Wang, et al., Energy Technol. 2 (2014) 159—165.
[115] S. Jaehee, H. Xiaogang, K.J. Gaskell, X. Kang, L. Sang Bok, H. Liangbing, J. Nanopart. Res. 16 (2014) 2745—2748.
[116] J.W. Kim, J.J. Travis, E. Hu, K.W. Nam, S.C. Kim, C.S. Kang, et al., J. Power Sources 254 (2014) 190—197.
[117] L. Xifei, L. Jian, M. Xiangbo, T. Yongji, M.N. Banis, Y. Jinli, et al., J. Power Sources 247 (2014) 57—69.
[118] H.-M. Cho, M.V. Chen, A.C. MacRae, Y.S. Meng, ACS Appl. Mater. Interfaces 7 (2015) 16231—16239.
[119] K. Jin Wook, K. Dong Hyeon, O. Dae Yang, L. Hyeyoun, K. Ji Hyun, L. Jae Hyun, et al., J. Power Sources 274 (2015) 1254—1262.
[120] J. Kang, B. Han, ACS Appl. Mater. Interfaces 7 (2015) 11599—11603.
[121] R.L. Patel, H. Xie, J. Park, H.Y. Asl, A. Choudhury, X. Liang, Adv. Mater. Interfaces 2 (2015) 1500046—1500054.
[122] J. Zhao, Y. Wang, Nano Energy 2 (2013) 882—889.
[123] J. Zhao, G. Qu, J.C. Flake, Y. Wang, Chem. Commun. 48 (2012) 8108—8110.
[124] Z. Jianqing, S. Aziz, W. Ying, J. Power Sources 247 (2014) 95—104.
[125] J.-Z. Kong, C. Ren, G.-A. Tai, X. Zhang, A.-D. Li, D. Wu, et al., J. Power Sources 266 (2014) 433—439.
[126] S. Aziz, J. Zhao, C. Cain, Y. Wang, J. Mater. Sci. Technol. 30 (2014) 427—433.
[127] J.S. Park, A.U. Mane, J.W. Elam, J.R. Croy, Chem. Mater. 27 (2015) 1917—1920.
[128] J. Xie, X. Yao, Q. Cheng, I.P. Madden, P. Dornath, C.-C. Chang, et al., Angew. Chem. Int. Ed. 54 (2015) 4299—4303.
[129] L.A. Riley, A.S. Cavanagh, S.M. George, Y.S. Jung, Y. Yan, S.-H. Lee, et al., ChemPhysChem 11 (2010) 2124—2130.
[130] D. Ahn, X. Xiao, Electrochem. Commun. 13 (2011) 796—799.
[131] A.C. Dillon, L.A. Riley, Y.S. Jung, C. Ban, D. Molina, A.H. Mahan, et al., Thin Solid Films 519 (2011) 4495—4497.
[132] Y. He, X. Yu, Y. Wang, H. Li, X. Huang, Adv. Mater. 23 (2011) 4938—4941.
[133] E. Kang, Y.S. Jung, A.S. Cavanagh, G.-H. Kim, S.M. George, A.C. Dillon, et al., Adv. Funct. Mater. 21 (2011) 2430—2438.
[134] I. Lahiri, S.-M. Oh, J.Y. Hwang, C. Kang, M. Choi, H. Jeon, et al., J. Mater. Chem. 21 (2011) 13621—13626.
[135] L.A. Riley, A.S. Cavanagh, S.M. George, S.-H. Lee, A.C. Dillon, Electrochem. Solid-State Lett. 14 (2011) A29—A31.
[136] X. Xiao, P. Lu, D. Ahn, Adv. Mater. 23 (2011) 3911—3915.
[137] E.L. Memarzadeh, W.P. Kalisvaart, A. Kohandehghan, B. Zahiri, C.M.B. Holt, D. Mitlin, J. Mater. Chem. 22 (2012) 6655—6668.
[138] W. Hsin-Yi, W. Fu-Ming, J. Power Sources 233 (2013) 1—5.
[139] J. Li, X. Xiao, Y.-T. Cheng, M.W. Verbrugge, J. Phys. Chem. Lett. 4 (2013) 3387—3391.
[140] A.J. Loebl, C.J. Oldham, C.K. Devine, B. Gong, S.E. Atanasov, G.N. Parsons, et al., J. Electrochem. Soc. 160 (2013) A1971—A1978.
[141] J.-G. Ren, Q.-H. Wu, G. Hong, W.-J. Zhang, H. Wu, K. Amine, et al., Energy Technol. 1 (2013) 77—84.
[142] T. Hu, M. Xie, J. Zhong, H.-t. Sun, X. Sun, S. Scott, et al., Carbon 76 (2014) 141—147.
[143] S.-Y. Kim, Y. Qi, J. Electrochem. Soc. 161 (2014) F3137—F3143.
[144] Y. Li, Y. Sun, G. Xu, Y. Lu, S. Zhang, L. Xue, et al., J. Mater. Chem. A 2 (2014) 11417—11425.
[145] A.L. Lipson, K. Puntambekar, D.J. Comstock, X. Meng, M.L. Geier, J.W. Elam, et al., Chem. Mater. 26 (2014) 935—940.
[146] E.M. Lotfabad, P. Kalisvaart, A. Kohandehghan, K. Cui, M. Kupsta, B. Farbod, et al., J. Mater. Chem. A 2 (2014) 2504—2516.
[147] T.Q. Nguyen, A.K. Thapa, V.K. Vendra, J.B. Jasinski, G.U. Sumanasekera, M.K. Sunkara, RSC Adv. 4 (2014) 3312—3317.
[148] D. Wang, J. Yang, J. Liu, X. Li, R. Li, M. Cai, et al., J. Mater. Chem. A 2 (2014) 2306—2312.
[149] J.C. Ye, Y.H. An, T.W. Heo, M.M. Biener, R.J. Nikolic, M. Tang, et al., J. Power Sources 248 (2014) 447—456.
[150] M. Yu, A. Wang, Y. Wang, C. Li, G. Shi, Nanoscale 6 (2014) 11419—11424.
[151] S. Hy, Y.-H. Chen, H.-M. Cheng, C.-J. Pan, J.-H. Cheng, J. Rick, et al., ACS Appl. Mater. Interfaces 7 (2015) 13801—13807.
[152] X. Kaiqi, H. Yu, B. Liubin, L. Hong, H. Xuejie, J. Power Sources 281 (2015) 455—460.
[153] A.C. Kozen, C.-F. Lin, A.J. Pearse, M.A. Schroeder, X. Han, L. Hu, et al., ACS Nano 9 (2015) 5884—5892.
[154] Q.-H. Wu, B. Qu, J. Tang, C. Wang, D. Wang, Y. Li, et al., Electrochim. Acta 156 (2015) 147—153.
[155] X. Han, Y. Xu, X. Chen, Y.-C. Chen, N. Weadock, J. Wan, et al., Nano Energy 2 (2013) 1197—1206.
[156] H. Kim, J.T. Lee, D.-C. Lee, A. Magasinski, W.-i. Cho, G. Yushin, Adv. Energy Mater. 3 (2013) 1308—1315.
[157] Y. Mingpeng, Y. Wenjing, L. Chun, H. Jong-Dal, S. Gaoquan, J. Mater. Chem. A 2 (2014) 7360—7366.
[158] M. Yu, A. Wang, F. Tian, H. Song, Y. Wang, C. Li, et al., Nanoscale 7 (2015) 5292—5298.
[159] C. Luo, J. Wang, X. Fan, Y. Zhu, F. Han, L. Suo, et al., Nano Energy 13 (2015) 537—545.
[160] Y. Xu, M. Zhou, X. Wang, C. Wang, L. Liang, F. Grote, et al., Angew. Chem. Int. Ed. 54 (2015) 8768—8771.
[161] L. Zhao, J. Zhao, Y.-S. Hu, H. Li, Z. Zhou, M. Armand, et al., Adv. Energy Mater. 2 (2012) 962—965.
[162] C. Guan, X. Wang, Q. Zhang, Z. Fan, H. Zhang, H.J. Fan, Nano Lett. 14 (2014) 4852—4858.
[163] L. Jian-Hong, H. Min-Hsiung, C. Yi-Wen, L. Ing-Chi, Appl. Phys. A 102 (2011) 545—550.
[164] E.M. Lotfabad, P. Kalisvaart, K. Cui, A. Kohandehghan, M. Kupsta, B. Olsen, et al., Phys. Chem. Chem. Phys. 15 (2013) 13646—13657.

[165] L. Meng-Lun, S. Chung-Yi, L. Yu-Hung, L. Shih-Chieh, C. Jin-Ming, P. Tsong-Pyng, et al., J. Power Sources 244 (2013) 410–416.
[166] M. Xie, X. Sun, C. Zhou, A.S. Cavanagh, H. Sun, T. Hu, et al., J. Electrochem. Soc. 162 (2015) A974–A981.
[167] W.-H. Ryu, J.-W. Jung, K. Park, S.-J. Kim, I.-D. Kim, Nanoscale 6 (2014) 10975–10981.
[168] B. Ahmed, D.H. Anjum, M.N. Hedhili, H.N. Alshareef, Small 11 (2015) 4341–4350.
[169] B. Ahmed, M. Shahid, D.H. Nagaraju, D.H. Anjum, M.N. Hedhili, H.N. Alshareef, ACS Appl. Mater. Interfaces 7 (2015) 13154–13163.
[170] N. Yesibolati, M. Shahid, W. Chen, M.N. Hedhili, M.C. Reuter, F.M. Ross, et al., Small 10 (2014) 2849–2858.
[171] A. Kohandehghan, P. Kalisvaart, K. Cui, M. Kupsta, E. Memarzadeh, D. Mitlin, J. Mater. Chem. A 1 (2013) 12850–12861.
[172] J. Liu, X. Li, M. Cai, R. Li, X. Sun, Electrochim. Acta 93 (2013) 195–201.
[173] B. Zhu, N. Liu, M. McDowell, Y. Jin, Y. Cui, J. Zhu, Nano Energy 13 (2015) 620–625.
[174] X. Han, Y. Liu, Z. Jia, Y.-C. Chen, J. Wan, N. Weadock, et al., Nano Lett. 14 (2014) 139–147.
[175] T. Aaltonen, M. Alnes, O. Nilsen, L. Costelle, H. Fjellvag, J. Mater. Chem. 20 (2010) 2877–2881.
[176] T. Aaltonen, O. Nilsen, A. Magrasó, H. Fjellvåg, Chem. Mater. 23 (2011) 4669–4675.
[177] J. Hamalainen, J. Holopainen, F. Munnik, T. Hatanpaa, M. Heikkila, M. Ritala, et al., J. Electrochem. Soc. 159 (2012) A259–A263.
[178] X. Li, J. Liu, M.N. Banis, A. Lushington, R. Li, M. Cai, et al., Energy Environ. Sci. 7 (2014) 768–778.
[179] J. Liu, M.N. Banis, X. Li, A. Lushington, M. Cai, R. Li, et al., J. Phys. Chem. C 117 (2013) 20260–20267.
[180] Y.-C. Perng, J. Cho, S.Y. Sun, D. Membreno, N. Cirigliano, B. Dunn, et al., J. Mater. Chem. A 2 (2014) 9566–9573.
[181] Y.S. Jung, A.S. Cavanagh, L. Gedvilas, N.E. Widjonarko, I.D. Scott, S.-H. Lee, et al., Adv. Energy Mater. 2 (2012) 1022–1027.
[182] S.H. Woo, H.-W. Lim, S. Jeon, J.J. Travis, S.M. George, S.-H. Lee, et al., J. Electrochem. Soc. 160 (2013) A2234–A2243.
[183] C. He, L. Qian, X. Qiang, Y. Yang, S. Zongping, W. Yong, J. Membr. Sci. 458 (2014) 217–224.
[184] M.Q. Snyder, S.A. Trebukhova, B. Ravdel, M.C. Wheeler, J. DiCarlo, C.P. Tripp, et al., J. Power Sources 165 (2007) 379–385.
[185] X. Sun, C. Zhou, M. Xie, T. Hu, H. Sun, G. Xin, et al., Chem. Commun. 50 (2014) 10703–10706.

Bilal Ahmed received his bachelor's degree in Materials Science and Engineering from Ghulam Ishaq Khan Institute of Science and Technology (GIKI), Pakistan in 2011. He earned master's degree in Advanced Energy Technology from University of Science and Technology, South Korea. In 2014, he joined Prof. Husam N. Alshareef's Group as Ph.D. student and currently working on two–dimensional materials for next generation secondary batteries.

Chuan Xia is currently a Ph.D. candidate of the Materials Science and Engineering program at KAUST in the group of Prof. Husam Alshareef. His research interests focus on the development of nanostructured materials and their applications in energy storage devices, including batteries, supercapacitors, and electrocatalysts.

Husam N. Alshareef is a Professor of Materials Science and Engineering at King Abdullah University of Science and Technology (KAUST), Saudi Arabia. He received his Ph.D. from North Carolina State University. He has worked as postdoctoral researcher at Sandia National Laboratory, followed by positions at Micron Technology, Inc. and Texas Instruments, Inc. His current research focuses on development of nanostructured materials for energy storage and electronic applications.

Please cite this article in press as: B. Ahmed, et al., Nano Today (2016), http://dx.doi.org/10.1016/j.nantod.2016.04.004